

1 Cost-benefit analysis of coastal flood defence measures in the North 2 Adriatic Sea

3 Mattia Amadio¹, Arthur H. Essenfelder¹, Stefano Bagli², Sepehr Marzi¹, Paolo Mazzoli², Jaroslav Mysiak¹,
4 Stephen Roberts³

5 ¹ *Centro Euro-Mediterraneo sui Cambiamenti Climatici, Università Ca' Foscari Venezia, Italy*

6 ² *Gecosistema, Rimini, Italy*

7 ³ *The Australian National University, Canberra, Australia*

8 *Correspondence to: Arthur H. Essenfelder (arthur.essenfelder@cmcc.it)*

9 Abstract

10 The combined effect of global sea levels rise and land subsidence phenomena poses a major threat to coastal
11 settlements. Coastal flooding events are expected to grow in frequency and magnitude, increasing the
12 potential economic losses and costs of adaptation. In Italy, a large share of the population and economic
13 activities are located along the low-lying coastal plain of the North Adriatic coast, one of the most sensitive to
14 relative sea level changes. Over the last half a century, this stretch of coast has experienced a significant rise in
15 relative sea level, the main component of which was land subsidence; in the forthcoming decades, climate-
16 induced sea level rise is expected to become the first driver of coastal inundation hazard. We propose an
17 assessment of flood hazard and risk linked with extreme sea level scenarios, both under historical conditions
18 and sea level rise projections at 2050 and 2100. We run a hydrodynamic inundation model on two pilot sites
19 located along the North Adriatic coast of Emilia-Romagna: Rimini and Cesenatico. Here, we compare
20 alternative extreme sea level scenarios accounting for the effect of planned and hypothetical seaside
21 renovation projects against the historical baseline. We apply a flood damage model to estimate the potential
22 economic damage linked to flood scenarios and we calculate the change in expected annual damage according
23 to changes in the relative sea level. Finally, damage reduction benefits are evaluated by means of cost-benefit
24 analysis. Results suggest an overall profitability of the investigated projects over time, with increasing benefits
25 due to increased probability of intense flooding in the next future.

26 **Key-words:** coastal inundation; extreme sea level; sea level rise; cost-benefit analysis; ANUGA; Italy

27 **Abbreviations:** MSL (Mean Sea Level); TWL (Total Water Level); ESL (Extreme Sea Level); SLR (Sea Level
28 Rise); VLM (Vertical Land Movements); DTM (Digital Terrain Model); EAD (Expected Annual Damage)

29 1. Introduction

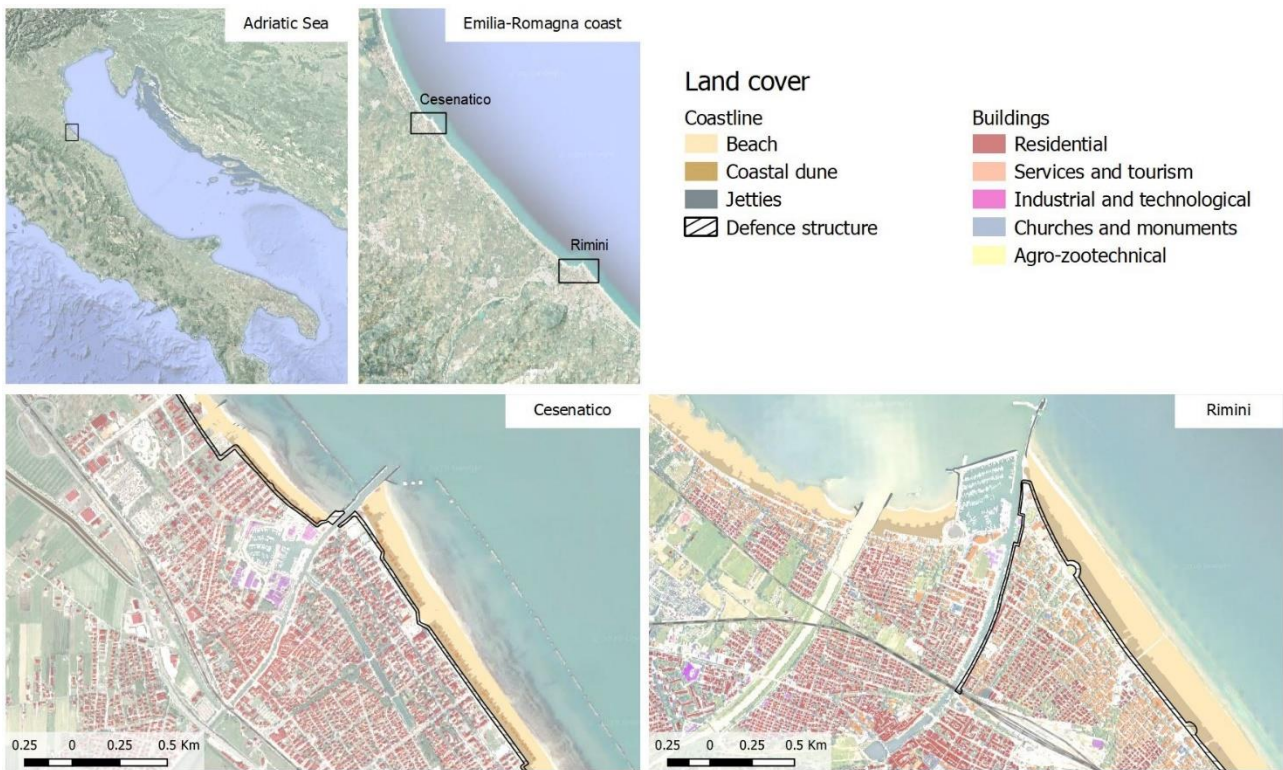
30 Globally, more than 700 million people live in low-lying coastal areas (McGranahan et al., 2007), and about
31 13% of them are exposed to a 100-year return period flood event (Muis et al., 2016). On average, one million
32 people located in coastal areas are flooded every year (Hinkel et al., 2014). Coastal flood risk shows an
33 increasing trend in many places due to socio-economic growth (Jongman et al., 2012b; Bouwer, 2011) and land
34 subsidence (Nicholls and Cazenave, 2010; Syvitski et al., 2009), but in the near future sea level rise (SLR) will
35 likely be the most important driver of increased coastal inundation risk (Hallegatte et al., 2013; Hinkel et al.,
36 2014). Evidences show that global sea level has risen at faster rates in the past century compared to the
37 millennial trend (Church and White, 2011; Kemp et al., 2011), topping 3.6 mm per year in the last decade (2006-
38 2015) mainly due to ocean thermal expansion and glacier melting processes (Meysignac and Cazenave, 2012;
39 Mitchum et al., 2010; Pörtner et al., 2019). According to the IPCC projections, it is very likely that, by the end
40 of the 21st century, the SLR rate will exceed that observed in the period 1971-2010 for all Representative
41 Concentration Pathway (RCP) scenarios (Pörtner et al., 2019); yet the local sea level can have a strong regional

42 variability, with some places experiencing significant deviations from the global mean change (Stocker et al.,
43 2013). This is particularly worrisome in regions where small changes in the mean sea level (MSL) can
44 drastically change the frequency of extreme sea level (ESL) events, leading up to situations where a 100-year
45 event may occur several times per year by 2100 (Vousdoukas et al., 2018, 2017; Carbognin et al., 2009, 2010;
46 Kirezci et al., 2020). Changes in the frequency of extreme events are likely to make existing coastal protection
47 inadequate in many places, causing a large part of the European coasts to be exposed to flood hazard. Under
48 these premises, coastal floods threaten to trigger devastating impacts on human settlements and activities
49 (McInnes et al., 2003; Lowe et al., 2001; Vousdoukas et al., 2017). In this context, successful coastal risk
50 mitigation and adaptation actions require accurate and detailed information about the characterisation of
51 coastal flood hazard and the performance of coastal defence options. Cost-benefit analysis (CBA) is widely
52 used to evaluate the economic desirability of a disaster risk reduction (DRR) project (Jonkman et al., 2004;
53 Price, 2018; Mechler, 2016), helping decision-makers in evaluating the efficacy of different adaptation options
54 (Kind, 2014; Bos and Zwaneveld, 2017).

55 In this study, we estimate the benefits of coastal renovation projects along the coast of Emilia-Romagna region
56 (Italy) in terms of avoided economic losses from ESL inundation events under both current and future
57 conditions. To do that, a range of hazard scenarios associated with ESL events are simulated over the two case
58 study areas: i) Rimini, a touristic hotspot that is currently implementing a seafront renovation project; and ii)
59 Cesenatico, a coastal city that could benefit from similar measures in addition to existing defence mechanisms.
60 The scenarios are designed by combining probabilistic data from historical ESL events with the estimates of
61 relative MSL change for those locations. Each scenario is evaluated in terms of direct economic impacts over
62 residential areas using a flood damage model. The combination of different risk scenarios in a CBA framework
63 allows to evaluate the economic profitability brought by the project implementation in terms of avoided losses
64 up to the end of the century.

65 **2. Area of study**

66 Located in the central Mediterranean Sea, the Italian peninsula has more than 8,300 km of coastline, hosting
67 around 18% of the country population, numerous towns and cities, industrial plants, commercial harbours
68 and touristic activities, as well as cultural and natural heritage sites. Existing country-scale estimates of SLR
69 impacts up to the end of this century helps to identify the most critically exposed coastal areas of Italy
70 (Antonioli et al., 2017; Marsico et al., 2017; Bonaduce et al., 2016; Lambeck et al., 2011). About 40% of the
71 country's coastal perimeter consist of a flat profile (ISPRA, 2012), potentially more vulnerable to the impacts
72 of ESL events. The North Adriatic coastal plain is the largest and most vulnerable location to extreme coastal
73 events due to the shape, morphology and low bathymetry of the Adriatic sea basin, which cause water level
74 to increase relatively fast during coastal storms (Perini et al., 2017; Ciavola and Coco, 2017; Carbognin et al.,
75 2010). Here the ESL is driven mainly by astronomical tide, ranging about one meter in the northernmost sector;
76 and by meteorological forcing, such as low pressure, seiches and prolonged rotational wind systems, which
77 are the main trigger of storm surge (Vousdoukas et al., 2017; Umgiesser et al., 2020). In addition to that, all the
78 coastal profile of the Padan plain shows relatively fast subsiding rates, partially due to natural phenomena,
79 but in large part linked to human activities (Perini et al., 2017; Carbognin et al., 2009; Meli et al., 2020). As a
80 contributing factor to coastal flood risk, the intensification of urbanization has led to increased exposure along
81 the Adriatic coast during the last 50 years, with many regions building over half of the available land within
82 300 meters from the shoreline (ISPRA, 2012). Figure 1 shows the location of the two case study areas,
83 Cesenatico and Rimini, along with land-cover maps showing the position of coastal defences accounted in this
84 study.



85

86

87

88

Figure 1. Case-study locations along the Emilia-Romagna coast: Cesenatico and Rimini. The coastal defence structure assessed in this study are shown in black. Buildings' footprint data from Regional Environmental Agency (ARPA) 2020. Basemap © Google Maps 2020.

89

The number of ESL events reported to cause impacts along the Emilia-Romagna coast shows a steady increase since the second half of the past century (Perini et al., 2011); this is partially explained by to the socio-economic development, which increased the extent of built-up asset potentially exposed to flood risk. The landscape along the 130 km regional coastline is almost completely flat, the only relief being old beach ridges, artificial embankments and a small number of dunes. The coastal perimeter is delineated by a wide sandy beach that is generally protected by offshore breakwaters, groins and jetties. The land elevation is often close to (or even below) the MSL, while the coastal corridor is heavily urbanised. Cesenatico has about 26,000 residents, while Rimini has 150,000. The towns have a strong touristic vocation, hosting large beach resort and bathing facilities along the beach and hundreds of hotels and rental housing located just behind the seaside. Both places have been affected by coastal storms resulting in flooding of buildings and activities, beach erosion and regression of the coastline. The most recent inundation events were observed in March 2010, November 2012 and February 2015. The 2015 event was one of the most severe ever recorded, with ESL values corresponding to a probability (return period) of once in 100 years. It caused severe damages along the whole regional coast and, in some locations, required the evacuation of people from their houses; many buildings and roads were covered by sand brought by the flood wave; touristic infrastructures near the shore were seriously damaged, and some port channels overflowed the surrounding areas. The economic impact of the event was estimated topping 7.5 M Eur (Perini et al., 2015).

106

3. Methodology

107

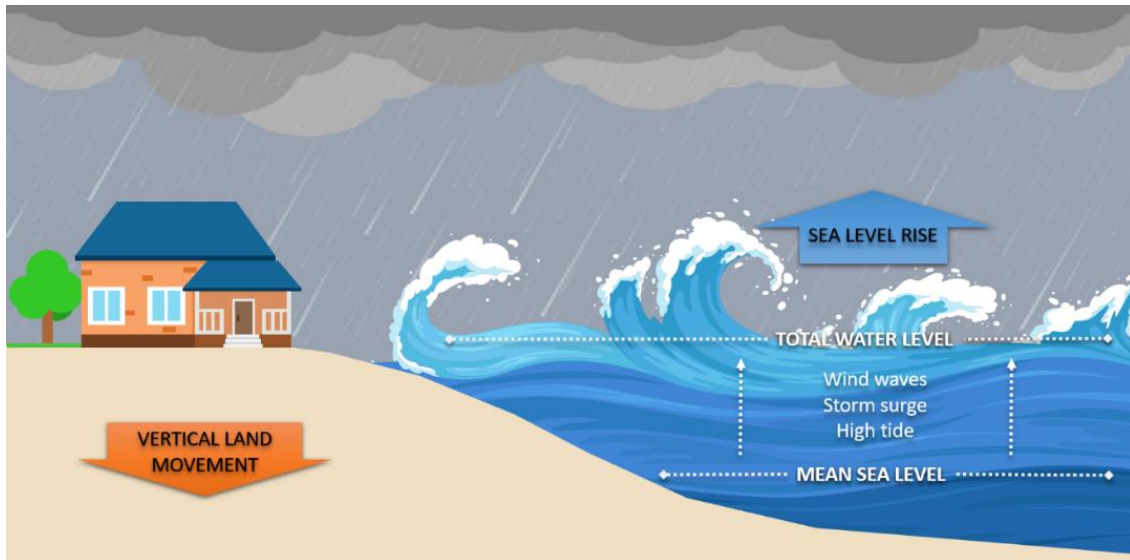
3.1 Components of the analysis

108

Coastal inundation is caused by an increase of total water level (TWL), most often associated to extreme sea level (ESL) events, which are often generated by a combination of high astronomical tide and meteorological

109

110 drivers such as storm surge and wind waves (Figure 2). Probabilistic flood risk assessments generally consider
111 ESL as the result of the combined effects of storm surge and tides (Muis et al., 2015; Vousdoukas et al., 2017).
112 More recent studies also account for the effects of waves by either adding wave setup to the ESL or by
113 simulating the dynamics of breaking waves on the coast (Kirezci et al., 2020; Melet et al., 2020; Li et al., 2020;
114 Wang et al., 2021; Muis et al., 2020; Lionello et al., 2021; McInnes et al., 2009; Idier et al., 2019). In our study,
115 we consider TWL near shore as the result of the combination of high tide, storm surge and action of waves,
116 the latter combining wave setup (defined as the increase of mean sea level at the shore that is caused by the
117 loss of wave momentum in the surf zone) with wave periodicity of incoming breaking waves (which defines
118 wave swash, i.e. the amplitude of the time varying elevation due to breaking waves along the shore).



119
120 **Figure 2.** Components of the analysis for extreme sea level events: total water level is the sum of maximum
121 tide, storm surge and wind waves over mean sea level. Vertical land movement and sea level rise affects the
122 mean sea level on the long run.

123 The identification of areas threatened by coastal flooding from ESL events is often done by means of flood
124 maps, which are generated through hydrostatic or hydrodynamic modelling approaches. These approaches
125 differ substantially in their complexity and their ability to represent environmental processes. The hydrostatic
126 inundation approach (sometimes referred as “bathtub”) is methodologically simple and computationally
127 quick, as it does not consider dynamic processes such as flow mass conservation and the effect of land cover
128 on the spread of floodwater, assuming flooded areas as those with an elevation below than a forcing water
129 level (Hinkel et al., 2010, 2014; Jongman et al., 2012b; Ramirez et al., 2016; Vousdoukas et al., 2016; Muis et al.,
130 2016). These assumptions and simplifications often result in substantial misestimation of flood extents
131 compared to the hydrodynamic flood modelling and observations (Bates et al., 2005; Vousdoukas et al., 2016;
132 Breilh et al., 2013; Ramirez et al., 2016; Seenath et al., 2016; Kumbier et al., 2019; Anderson et al., 2018). To
133 overcome these limitations, hydrodynamic flood modelling approaches capable of accounting for the effects
134 of wind, waves, tide, current, and river run-off can be used (Barnard et al., 2019). The most advanced models
135 can simulate atmospheric–ocean–land interactions from the deep ocean to the coast with a satisfactory
136 predictive skill (Bates et al., 2005; Seenath et al., 2016; Vousdoukas et al., 2016; Lewis et al., 2013), at the costs
137 of a more complex model setup, extensive data requirements and significantly longer computational times
138 (Teng et al., 2017). As intermediate solution, simplified hydrodynamic flood models that focus on nearshore
139 processes are capable of reducing the computational cost while taking into consideration water mass
140 conservation (Breilh et al., 2013), aspects of flooding hydrodynamics (Dottori et al., 2018) and the presence of
141 obstacles (Perini et al., 2016). They proved to be reliable for coastal flooding applications, such as the

142 simulation of coastal flooding due to storm-tide events (Ramirez et al., 2016; Bates et al., 2005; Skinner et al.,
143 2015; Smith et al., 2012).

144 In this study, estimates of ESL components (storm surge, tides and waves) are obtained for the North Adriatic
145 up to year 2100 by combining reference hazard scenarios derived from the analysis of historical records (Perini
146 et al., 2011, 2016, 2017; Armaroli et al., 2012; Armaroli and Duo, 2018) with regionalised projections of SLR
147 (Vousdoukas et al., 2017) and local vertical land movements (VLM) rates (Perini et al., 2017; Carbognin et al.,
148 2009). On this basis, four hypothetical ESL scenarios are designed, ranging from low intensity-high frequency
149 to high intensity-low frequency, under both current and future (2050 and 2100) conditions. The hydrodynamic
150 model ANUGA (Roberts et al., 2015) is applied to simulate the inundation of land areas during ESL accounting
151 for individual components. Land morphology and exposure of coastal settlements are described by high-
152 resolution DTM (LiDAR) and bathymetry, in combination with land use and buildings footprints. The effect
153 of hazard mitigation structures (both designed and under construction) are explicitly accounted by the model
154 in the “defended” scenario, in contrast to the baseline scenario, where only existing defence structures (groins,
155 jetties, breakwaters and sand dunes) are considered.

156 3.2 Vertical Land Movement

157 Vertical land movements result from a combination of slow geological processes such as tectonic activity and
158 glacial isostatic adjustment (Peltier et al., 2015; Peltier, 2004), and medium-term phenomena, such as sediment
159 loading and soil compaction (Carminati and Martinelli, 2002; Lambeck and Purcell, 2005). The latter can
160 greatly oversize geological processes at local scale (Wöppelmann and Marcos, 2012); in particular, faster
161 subsidence occurs in presence of intense anthropogenic activities such as water withdrawal and natural gas
162 extraction (Teatini et al., 2006; Polcari et al., 2018). Most of the peninsula shows a slow subsiding trend,
163 although with some local variability. An estimate of VLM rates due to tectonic activity has been derived from
164 studies conducted in Italy (Solari et al., 2018; Antonioli et al., 2017; Marsico et al., 2017; Lambeck et al., 2011).
165 The North Adriatic coastal plain shows the most intense long-term geological subsidence rates (about 1 mm
166 per year), increasing North to South. Yet in the last decades these rates were often greatly exceeded by ground
167 compaction rates observed by multi-temporal SAR Interferometry (Gambolati et al., 1998; Antonioli et al.,
168 2017; Polcari et al., 2018; Solari et al., 2018). Observed subsidence is about one order of magnitude faster where
169 the aquifer system has been extensively exploited for agricultural, industrial and civil use since the post-war
170 industrial boom. From the 1970s, however, with the halt of groundwater withdrawals, anthropogenic drivers
171 of subsidence has been strongly reduced or stopped (Carbognin et al., 2009). Nonetheless, subsidence still
172 continues at much faster rates than expected from natural phenomena (Teatini et al., 2005). Geodetic surveys
173 carried out from 1953 to 2003 along the Ravenna coast provide evidence of a cumulative land subsidence
174 exceeding 1 m at some sites due to gas extraction activities. Average subsidence rates observed for 2006-2011
175 along the Emilia-Romagna coast are around 5 mm/yr, exceeding 10 mm/yr in the back shore of the Cesenatico
176 and Rimini areas and topping 20-50 mm/yr in Ravenna (Perini et al., 2017; Carbognin et al., 2009). Based on
177 these current rates, we assume an average fixed annual VLM of 5 mm in both Cesenatico and Rimini up to the
178 end of the century. This remarkable difference between natural VLM rates and observations would produce a
179 dramatic effect on the estimated SLR scenarios: at present rates, Rimini would see an increase of MSL by 0.15
180 m in 2050 and more than 0.4 m in 2100 independently from eustatic SLR. Since these rates are connected with
181 human activity, it is not possible to foresee how they will change in the longer run.

182 3.3 Sea Level Rise

183 The long availability of tide gauge data along the North Adriatic coast allows to assess the changes in MSL
184 during the last century, estimated to be +1.3 mm/year (Scarascia and Lionello, 2013). This is consistent with

185 published values for the Mediterranean Sea (Tsimplis et al., 2008; Tsimplis and Rixen, 2002) and the Adriatic
186 Sea (Tsimplis et al., 2012; Carbognin et al., 2009). The projections of future MSL account for sea thermal
187 expansions from four global circulation models, estimated contributions from ice-sheets and glaciers (Hinkel
188 et al., 2014) and long-term subsidence projections (Peltier, 2004). The ensemble mean is chosen to represent
189 each RCP for different time slices. The increase in the central Mediterranean basin is projected to be
190 approximately 0.2 m by 2050 and between 0.5 and 0.7 m by 2100, compared to historical mean (1970-2004)
191 (Vousdoukas et al., 2017). As agreed with local stakeholders (*Comune di Rimini*), our analysis considers the
192 intermediate emission scenario RCP 4.5, projecting an increase in MSL of 0.53 m at 2100. It must be noted that
193 these projections, although downscaled for the Adriatic basin, do not account for the peculiar continental
194 characteristics of the shallow northern Adriatic sector, where the hydrodynamics and oceanographic
195 parameters partially depend on the freshwater inflow (Zanchettin et al., 2007).

196 3.4 Tides and meteorological forcing

197 Storm surge and wind waves represent the largest contributions to TWL during an ESL event. An estimation
198 of these components is obtained for the two coastal sites from the analysis of tide gauge and buoy records,
199 and from the description of historical extreme events presented in local studies (Armaroli and Duo, 2018;
200 Perini et al., 2012; Masina et al., 2015; Perini et al., 2011, 2017). This area is microtidal: the mean neap tidal
201 range is 30–40 cm, and the mean spring tidal range is 80–90 cm. Most storm surge events have a duration of
202 less than 24 h and a maximum significant wave height of about 2.5 m. During extreme cyclonic events, the
203 sequence of SE wind (*Sirocco*) piling the water North and E-NE wind (*Bora*) pushing waves towards the coast
204 can generate severe inundation events, with significant wave height ranging 3.3 – 4.7 m and exceptionally
205 exceeding 5.5 m (Armaroli et al., 2012). Fifty significant events have been recorded from 1946 to 2010 on the
206 ER coast, with half of them causing severe impacts along the whole coast and 10 of them being associated with
207 important flooding events (Perini et al., 2017). The most severe events are found when strong winds blow
208 during exceptional tide peaks, most often happening in late autumn and winter. The event of November 1966
209 represents the highest ESL on records, causing significant impacts along the regional coast: the recorded water
210 level was 1.20 m above MSL, and wave heights offshore were estimated around 6–7 m (Garnier et al., 2018;
211 Perini et al., 2011). The whole coastline suffered from erosion and inundation, especially in the province of
212 Rimini. Atmospheric forcing shown significant variability for the period 1960 onwards (Tsimplis et al., 2012),
213 but there is no strong evidence supporting a significant change in marine storminess frequency or severity for
214 the near future (Lionello, 2012; Zanchettin et al., 2020; Lionello et al., 2020, 2017). Thus, in our model we assume
215 meteorological forcing to remain the same up to 2100.

216 3.5 Terrain morphology and coastal defence structures

217 Reliable bathymetry and topography are required in order to run the hydrodynamic modelling at the local
218 scale. Bathymetric data for the Mediterranean Sea were obtained from the European Marine Observation and
219 Data Network (EMODnet) at 100 m resolution. The description of terrain morphology comes from the official
220 high-resolution LiDAR DTM (MATTM, 2019). First, we combined the coastal dataset (2 m resolution and
221 vertical accuracy of ± 0.2 m), and the inland dataset (1 m resolution and vertical accuracy ± 0.1 m) into one
222 seamless layer. Then, the DTM is supplemented with geometries of existing coastal protection elements such
223 as jetties, groins and breakwaters obtained from the digital Regional Technical Map. In Rimini, the *Parco del*
224 *Mare* (Figure 3) is an urban renovation project which aims to improve the seafront promenade: the existing
225 road and parking lots are converted into an urban green infrastructure consisting of a concrete barrier covered
226 by vegetated sandy dunes with walking paths. This project also acts as a coastal defence system during
227 extreme sea level events. The barrier rises 2.8 meters along the southern section of the town, south of the

228 marina; no barrier is planned on the northern coastal perimeter. The *Parco del Mare* project is expected to be
229 completed by 2021 and has been taken in account in the evaluation of the “defended” scenarios by adding the
230 barrier elevation to the DTM.



231
232 **Figure 3.** Prototype design of Parco del Mare project in Rimini. Adapted from JDS Architects.

233 In Cesenatico, the existing defence structures include a moving barrier system (*Porte Vinciane*) located on the
234 port channel, coupled with a dewatering pump which discharge the meteoric waters in the sea. The barriers
235 close automatically if the TWL surpasses 1 meter over the mean sea level, preventing floods in the historical
236 centre up to 2.2 meters of TWL. Additional defence structures include the winter dunes, which consist of a 2.2
237 meter-tall intermittent, non-reinforced sand barrier. In the defended scenario, we envisage a coastal defence
238 structure similar to Rimini’s *Parco del Mare* project, spanning both North and South of the port channel with a
239 total length of 7.8 km. The DTM was manually edited based on additional reference data (i.e. on-site
240 observations or aerial photography) in order to remove artefacts and to produce a more realistic representation
241 of the land morphology. Bridges and tunnels are the most critical elements that required DTM correction in
242 order to avoid misrepresentations of the water flow routing.

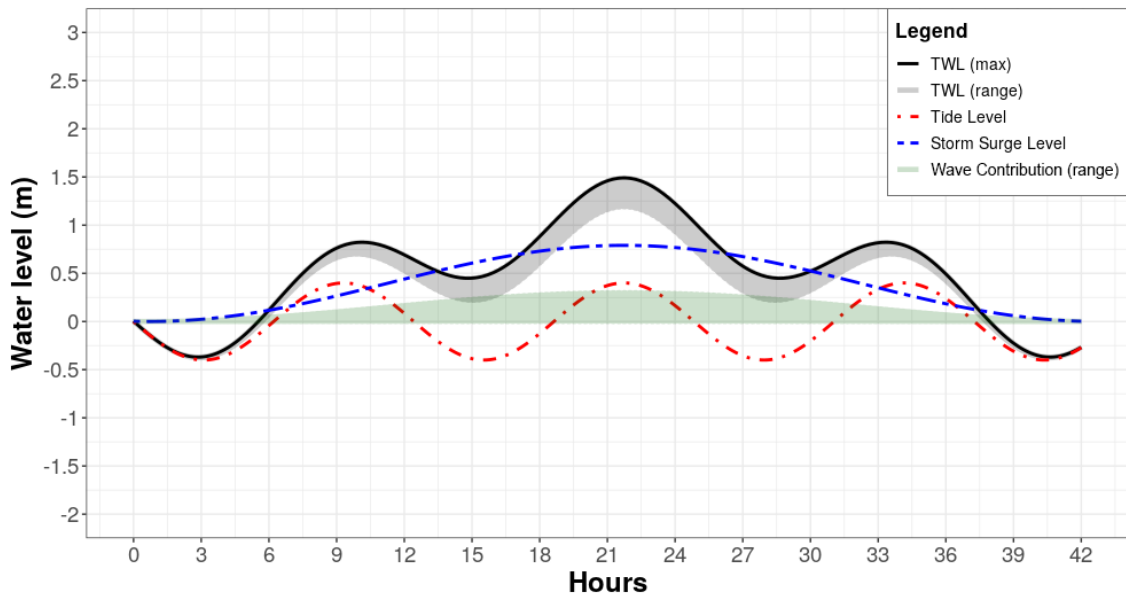
243 3.6 Scenario design

244 In order to design probabilistic nearshore scenarios associated to ESL of different intensities to use as boundary
245 conditions in the hydrodynamic model, we rely on existing analysis of ESL events occurring on the regional
246 coast (Perini et al., 2011, 2016, 2017), which have been adopted by the Regional Environmental Agency to
247 define the official coastal flood hazard zones and related protection standards (ARPA Emilia-Romagna, 2019).
248 The probability of occurrence of these ESL scenarios is expressed in terms of return period (*RP*), which is the
249 estimated average time interval (in years) between events of similar intensity. Four scenarios of increasing
250 intensity are designed, namely *RP 1, 10, 100* and *250* years. For each of these hypothetical scenarios, the TWL
251 nearshore is calculated as the sum of extreme values for storm surge level (*SS*), max tide (*T_{max}*) and wave
252 contribution (*W_c*) at each time-step (see Table 1). In particular, given the limitation of the considered 2D
253 hydrodynamic model in not resolving vertical convection and waves breaking (i.e. swash), we include wave
254 contribution to TWL by accounting for wave setup (*W_s*) with a periodicity equal to the incoming breaking
255 waves (*W_p*), thus partially representing wave motion (Armaroli et al., 2012, 2009). We develop a set of
256 trigonometric equations based on harmonic analysis concepts to characterise the amplitude and period of
257 tidal, storm surge, and wave levels as the harmonics constituents that describe the theoretical temporal
258 evolution of the nearshore TWL during an ESL event (see Figure 4). Harmonics constituents are the elements
259 in a mathematical expression of a series of periodic terms and have been used in harmonic analysis for sea
260 level prediction (Boon, 2011; Familkhalili et al., 2020; Fuhrmann et al., 2019; Annunziato and Probst, 2016). The
261 set of equations used in the study are specified in Appendix A, together with sample applications and
262 validation metrics to observed ESL events along the coast of ER. Additional variables to characterize the event

263 dynamics are the storm surge duration (*Time*, in hours) and the wave period (*Wp*, in seconds), both obtained
 264 from regional studies of ESL events (Armaroli et al., 2012; Armaroli and Duo, 2018). Projections of TWL at
 265 2050 and 2100 are calculated for the same set of RP scenarios by adding SLR and VLM contributions to the
 266 MSL, thus shifting the TWL curve up by 33 cm in 2050 and by 97 cm in 2100.

267 **Table 1.** components of nearshore TWL for four ESL scenarios (RPs) designed according to analysis of
 268 historical ESL events and projected MSL change (2050 and 2100), accounting for both SLR (RCP 4.5) and
 269 average VLM rate.

RP (years)	Extreme event features					Historical	2050			2100		
	SS (m)	T _{max} (m)	Ws (m)	Time (h)	Wp (s)	TWL (m)	SLR (m)	VLM (m)	TWL (m)	SLR (m)	VLM (m)	TWL (m)
1	0.60	0.40	0.22	32	7.7	1.22	0.14	0.19	1.55	0.53	0.44	2.19
10	0.79	0.40	0.30	42	8.9	1.49	0.14	0.19	1.82	0.53	0.44	2.46
100	1.02	0.40	0.39	55	9.9	1.81	0.14	0.19	2.14	0.53	0.44	2.78
250	1.40	0.45	0.65	75	11	2.50	0.14	0.19	2.83	0.53	0.44	3.47



Source: Authors' elaboration

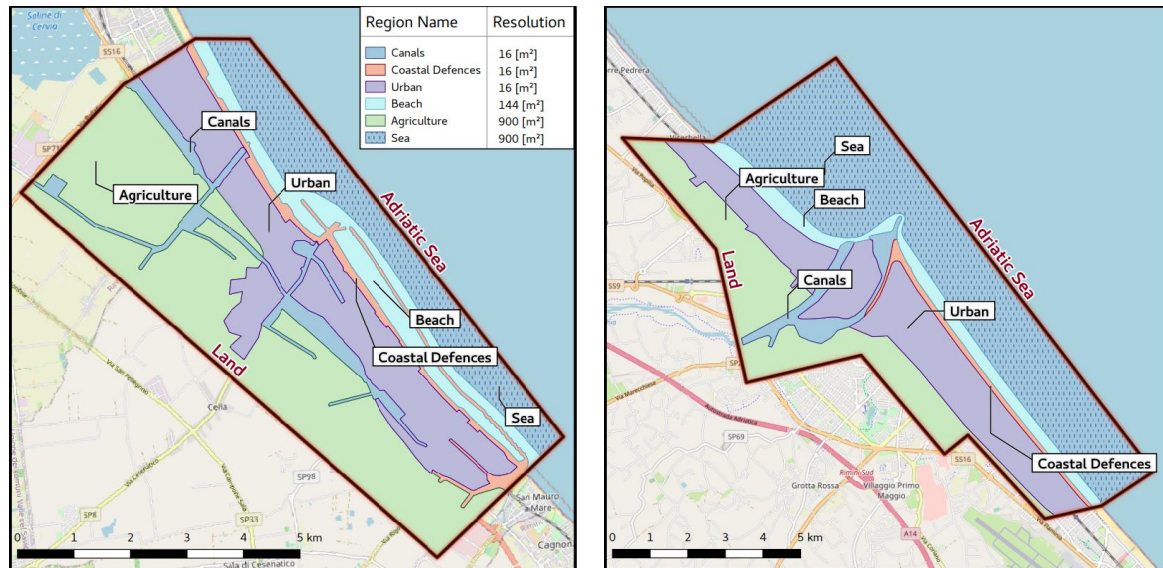
270 **Figure 4.** Design of dynamic ESL scenario corresponding to RP 10 years under historical MSL conditions. The
 271 maximum TWL is shown as the black continuous line, while TWL range at any given time is shown as the
 272 shaded grey area. The components of the nearshore TWL are the tide level (red dashed line), the storm surge
 273 level (blue dashed line) and the waves contribution (green shaded area). Waves contribution is represented as
 274 a shaded area due to its high frequency (period of 8.9s). In this scenario (RP 10) the maximum storm surge
 275 level is 0.79 m, the maximum high tide is 0.40 m, and the wave contribution ranges from 0.00 m to 0.30 m, with
 276 a wave period of 8.9 seconds. At the peak of the event, these conditions produce a maximum TWL of 1.49 m.
 277

278 Figure 5 shows how the nearshore TWL results at any given time from the combination of storm surge, tide
 279 level and wave contribution in the scenario RP 10 years (additional figures for all RP scenarios can be found
 280 in Appendix A). The individual contribution of *SS* and *T_{max}* levels are represented by coloured dashed lines
 281 in the figure. The *Wc* component is shown as a green shaded area due to its high frequency (defined by the
 282 wave period, *Wp*, in seconds), thus representing the range of values assumed in any given time. The intensity
 283 of wave contribution to ESL is assumed to grow proportionally to the increase of the *SS* component. The
 284 shaded grey area represents the range of TWL as sum of these components, while the black continuous line
 285 represents the maximum TWL at any given time. Our approach is precautionary as it provides worst-case

286 TWL values: SS peak is set to coincide with T_{max} and W_c at the mid of the event, thus resulting in the
 287 maximum TWL possible under each scenario.

288 3.7 Inundation modelling

289 The nearshore ESL scenarios specified in Table 1 and exemplified in Figure 4 (and Appendix A) are used as
 290 forcing boundary condition in ANUGA, a 2D hydrodynamic model suitable for the simulation of flooding
 291 resulting from riverine peak flows and storm surges (Roberts, 2020). The fluid dynamics simulation is based
 292 on a finite-volume method for solving the shallow water wave equations, thus being based on continuity and
 293 simplified momentum equation. Being a 2D hydrodynamic model, ANUGA does not resolve vertical
 294 convection, waves breaking or 3D turbulence (i.e. vorticity), thus it cannot account for the swash component
 295 of wave runup. Wave direction is set to be oriented perpendicular to the coast. For each scenario, ANUGA
 296 computes the TWL on the coast, the resulting water depth of inundation, and the horizontal momentum on
 297 an unstructured triangular grid (mesh) representing the two case study areas. The size of the triangles is
 298 variable within the mesh, thus allowing for a better representation in regions of particular interest, such as
 299 along the coastline, in urban areas, and inside the canals. Six different regions are used in each case study to
 300 define different triangular mesh resolution, varying from higher resolution areas of 16 m² for canals and
 301 coastal defence structures, to lower resolution of 900 m² for sea areas. The output of the simulation consists of
 302 maps representing flood extent, water depth and momentum at every time step (~1 second), projected on the
 303 high-resolution DTM grid (1 meter). Figure 6 presents the two case study areas and the respective resolutions
 304 for each region. The resulting irregular mesh counts with about 637 thousand triangles for the Cesenatico
 305 domain, and about 1,2 million triangles for the Rimini domain. The model includes an operator module that
 306 simulates the removal of sand associated with over-topping of a sand dune by sea waves. The operator
 307 simulates the erosion, collapse, fluidisation and removal of sand from the dune system (Kain et al., 2020). This
 308 option is enabled only in the undefended scenario for Cesenatico, where non-reinforced sand dunes are prone
 309 to erosion.



310
 311 **Figure 5.** The definition of simulation domain for the cities of Cesenatico (on the left) and Rimini (on the right).
 312 The legend shows the mesh resolution specific to each region simulated by the model.

313 3.8 Risk modelling and Expected Annual Damage

314 Direct damage to physical asset is estimated using a customary flood risk assessment approach originally
 315 developed for fluvial inundation, which is adapted to coastal flooding assuming that the dynamic of impact

316 from long-setting floods depends on the same factors, namely: 1) hazard magnitude, and 2) type, size and
 317 value of exposed asset. Indirect economic losses due to secondary effects of damage (e.g. business interruption)
 318 are excluded from the computation. Hazard magnitude can be defined by a range of variables, but the most
 319 important predictors of damage are water depth and the extension of the flood event (Jongman et al., 2012a;
 320 Huizinga et al., 2017). The characterization of exposed asset is built from a variety of sources, starting from
 321 land use and buildings footprints obtained from the Regional Environmental Agencies geodatabases and the
 322 Open Street Map database (Open Street Map data for Nord-Est Italy, 2019). Additional indicators about
 323 buildings characteristics are obtained from the database of the 2011 Italian Census (15° censimento della
 324 popolazione e delle abitazioni, 2019), while mean construction and restoration costs per building types are
 325 obtained from cadastral estimates (CRESME, 2019). The asset representation is static, thus not accounting for
 326 changes in land use nor population density, while allowing for the direct comparison of hazard mitigation
 327 options' results. A depth-damage function validated on empirical records (Amadio et al., 2019) is applied in
 328 order to translate each hazard scenario into an estimate of economic risk, measured as a share of total exposed
 329 value. The damage function applies only to residential and mixed-residential buildings, the area of which
 330 represents about 93% of total exposed footprints; other types (such as harbour infrastructures, industrial,
 331 commercial, historical monuments and natural sites) are excluded from risk computation. Abandoned or
 332 under-construction buildings are also excluded from the analysis. To avoid overcounting of marginally-
 333 affected buildings, we set two threshold conditions for damage calculation: flood extent must be greater than
 334 or equal to 10 m², and maximum water depth must be greater than or equal to 10 cm. The damage/probability
 335 scenarios are combined together as Expected Annual Damage (EAD). EAD is the damage that would occur in
 336 any given year if damages from all flood probabilities were spread out evenly over time; mathematically, EAD
 337 is the integration of the flood risk density curve over all probabilities (Olsen et al., 2015), as in equation 1.

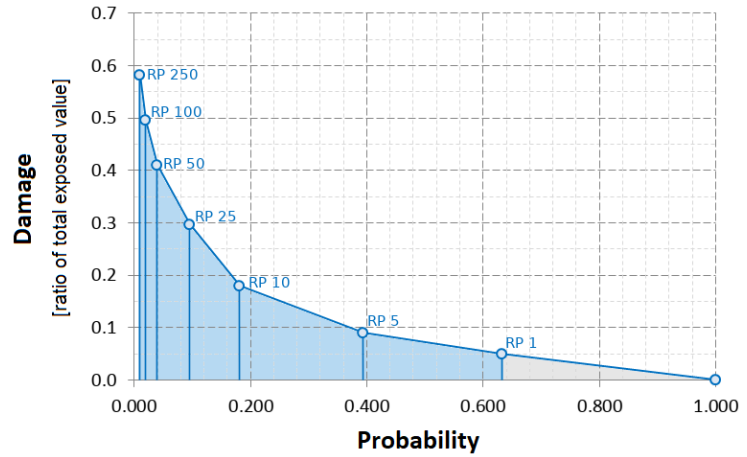
$$EAD = \int_0^1 D(p) dp \quad (1)$$

338 The integration of the curve can be solved either analytically or numerically, depending on the complexity of
 339 the damage function $D(p)$. Several different methods for numerical integration exist; we use an approach
 340 where EAD is the sum of the product of the fractions of exceedance probabilities by their corresponding
 341 damages (Figure 7). We calculate $D(p)$, which is the damage that occurs at the event with probability p , by
 342 using the depth-damage function for each hazard scenario. The exceedance probability of each event (p) is
 343 calculated based on exponential function as shown in equation 2.

$$p = 1 - e^{\left(\frac{-1}{RP}\right)} \quad (2)$$

344 Events with a high probability of occurrence and low intensity (below RP 1 year) are not simulated, as they
 345 are assumed to not cause significant damage. This is consistent with the historical observations for the case
 346 study area, although this assumption could change with increasing MSL.

Figure 6. Schematic representation of the numerical integration of the damage function $D(p)$ with respect to the exponential probability of the hazard events. Damage (Y axis) represents the ratio of damage to the total exposed value estimated up to the most extreme scenario (RP 250 years). Events with a probability of occurrence higher than once in a year are expected to not cause damage (grey area).



347 3.9 Cost-Benefit Analysis

348 A CBA should include a complete assessment of the impacts brought by the implementation of the hazard
 349 mitigation option, i.e. direct and indirect, tangible and intangible impacts (Bos and Zwaneveld, 2017). The
 350 project we are considering, however, has not been primarily designed for DRR purpose: instead, it is meant
 351 as an urban renovation project which aims to consolidate the touristic vocation of the area, to improve the
 352 quality of life and the urban environment (Comune di Rimini, 2018). This implies some large indirect effects
 353 on the whole area, most of which are not strictly related to disaster risk management and, overall, very difficult
 354 to estimate ex-ante. Our evaluation focuses only on the benefits that are measurable in terms of direct flood
 355 losses reduction. Regarding the implementation costs, the CBA accounts for the initial investment required
 356 for setting up the adaptation measure, and operational costs through time. According to the *Parco del Mare*
 357 project funding documentation (Comune di Rimini, 2019b, a, 2020, 2021a, b), the total cost of the project (to be
 358 completed during 2021) is 33.3 M Eur, corresponding to 5.55 M Eur per Km of length. No information is
 359 available about maintenance costs of the opera, but given the nature of the project (static defense with low
 360 structural fragility), we assume they will be rather small compared to the initial investment. Ordinary annual
 361 maintenance costs are accounted as 0.1% of the total cost of the project. The same costs are assumed for the
 362 hypothetical barrier in Cesenatico, resulting in an initial investment cost of 43.3 M. Costs and benefit occurring
 363 in the future periods need to be discounted, as people put higher value on the present (Rose et al., 2007). This
 364 is done by adjusting future costs and benefits using an annual discount rate (r). We chose a variable rate of $r =$
 365 3.5 for the first 50 years and $r = 3$ from 2050 onward (Lowe, 2008). A sensitivity analysis of discount rate is
 366 included in Appendix B. The three main decision criteria used in CBA for project evaluation are the Net
 367 Present Value (NPV), the Benefit/Cost Ratio (BCR) and the payback period. The NPV is the sum of Expected
 368 Annual Benefits (B) up to the end of the time horizon, discounted, minus the total costs for the implementation
 369 of the defense measure, which takes into account initial investment plus discounted annual maintenance costs
 370 (C). In other words, the NPV of a project equals the present value of the net benefits ($NB_i = B_i - C_i$) over a period
 371 of time (Boardman et al., 2018), as in equation 3:

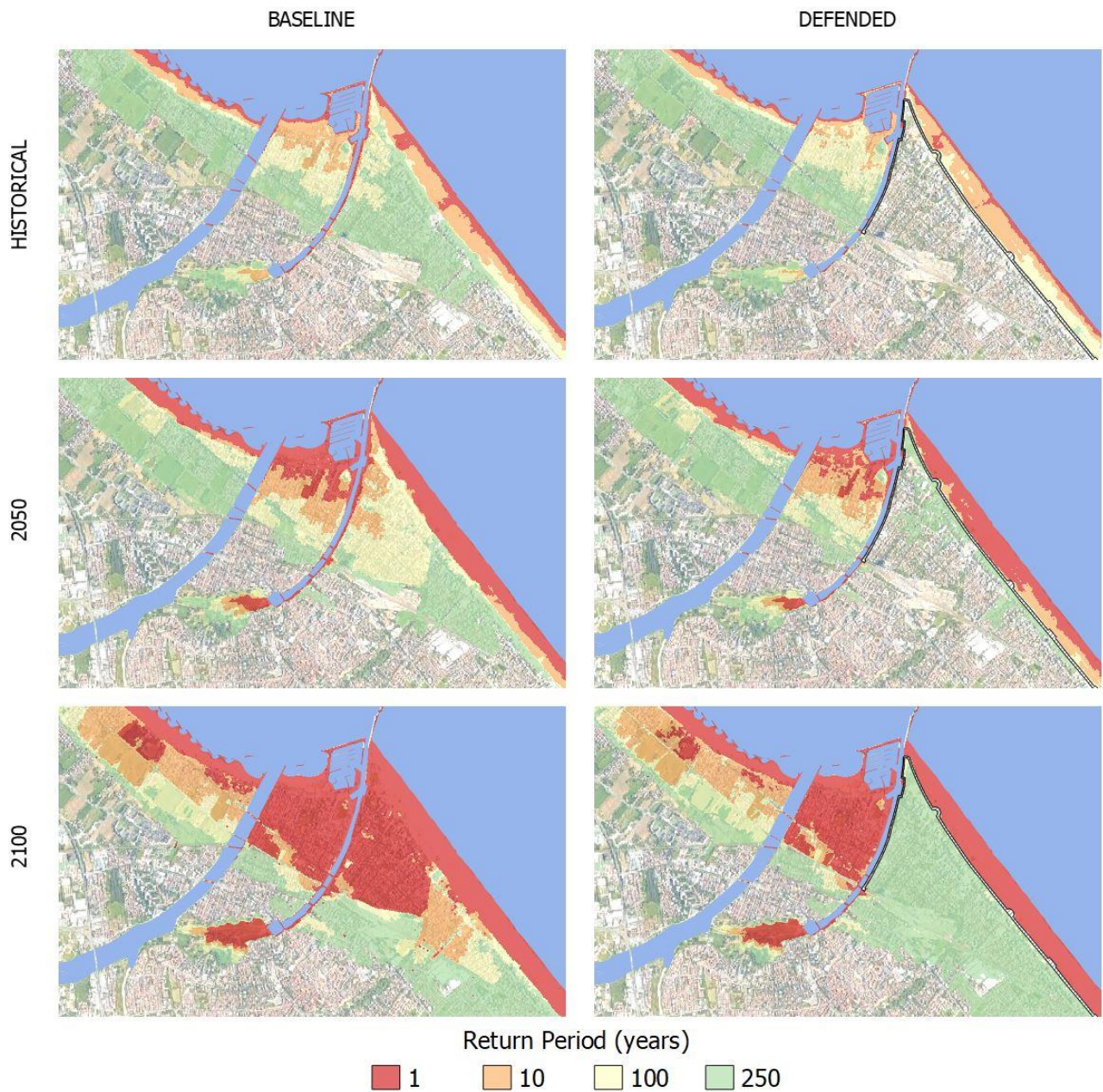
$$NPV = PV(B) - PV(C) = \sum_{t=0}^n \frac{NB_t}{(1+r)^t} \quad (3)$$

372 Positive NPV means that the project is economically profitable. The BCR is instead the ratio between the
 373 benefits and the costs; a BCR larger than 1 means that the benefits of the project exceed the costs on the long
 374 term and the project is considered profitable. The payback period is the number of years required for the
 375 discounted benefits to equal the total costs.

376 **4. Results**

377 **4.1 Inundation scenarios**

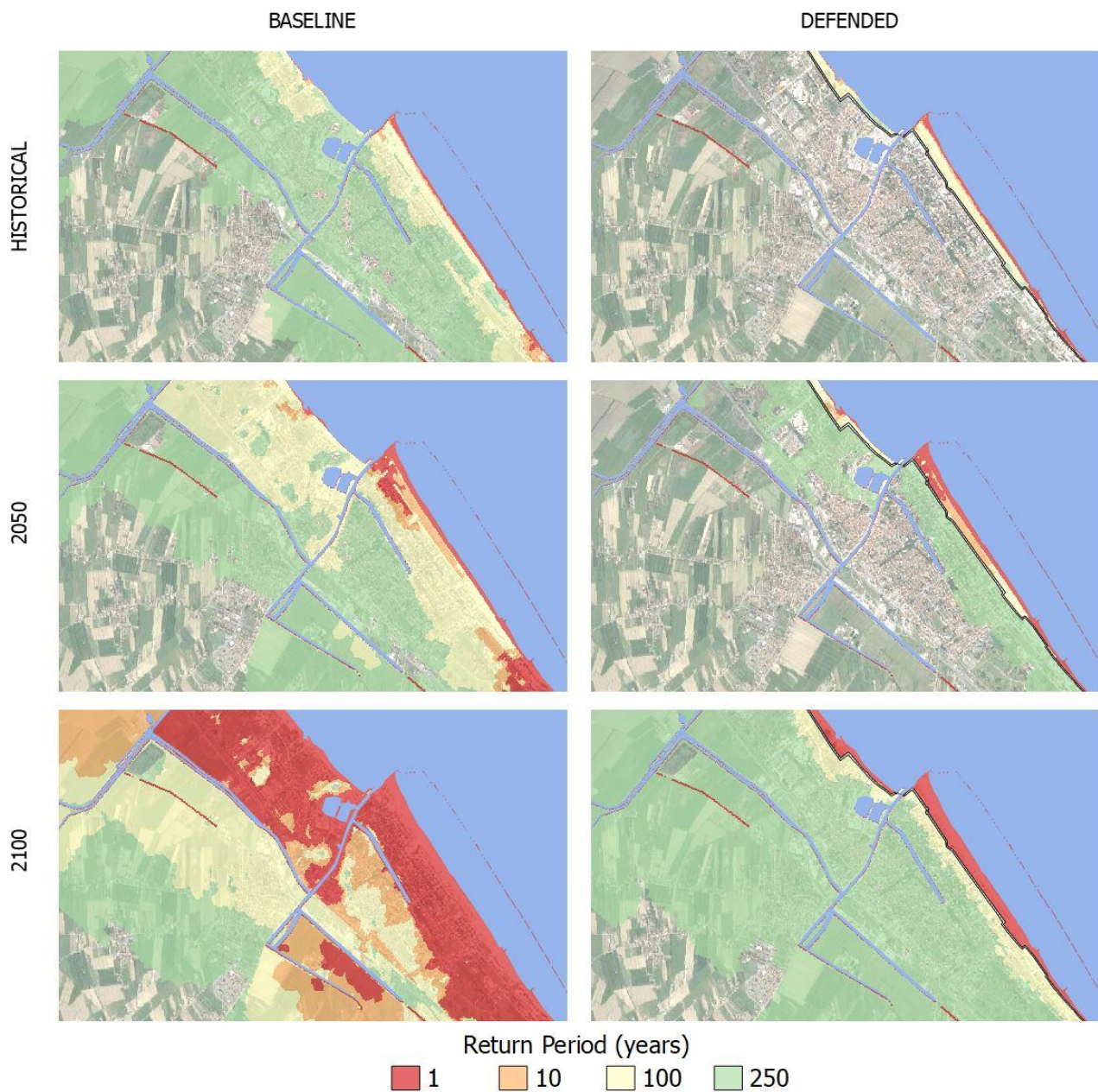
378 Once the setup is completed, the hydrodynamic model performs relatively fast: each simulation is carried at
379 half speed compared to real time, requiring about 24 hours to simulate a 12 h event. Parallel simulations for
380 the same area can run on a multicore processor, improving the efficiency of the process. The output of the
381 hydrodynamic model consists of a set of inundation simulations that include several hazard intensity variables
382 in relation to flood extent: water depth, flow velocity, and duration of submersion. ESL scenarios are then
383 summarized into static maps, each one representing the maximum value reached by hazard intensity variables
384 during the simulated event at about 1 meter resolution. The flood extents corresponding to each RP scenario
385 are shown for Rimini (Figure 8) and Cesenatico (Figure 9).



386

387 **Figure 7.** Rimini, extent of land affected by flood according to frequency of occurrence of ESL event up to 2100
388 for the baseline [left] and the defended scenario [right]. Basemap © Google Maps 2020.

389 In Rimini, the *Parco del Mare* barrier produces benefits in terms of avoided flooding in the south-eastern part
 390 of the town (high-density area) for ESL events with a return period of 100 years or less. The north-western part
 391 and the marina are outside of the defended area; these areas are therefore subject to a similar amount of
 392 flooding across scenarios. In all the simulations, the buildings located behind the marina are the firsts to be
 393 flooded. In fact, the new and the old port channels located on both sides of the marina represent a hazard
 394 hotspot: as shown in the maps, the failure of the eastern channel, which has a relatively low elevation, is likely
 395 to cause the water to flood the eastern part of the town, even during inundation events that would not surpass
 396 the beach. In the defended scenarios, where both the coastal and the canal barriers are enabled, the flood extent
 397 in the south-eastern urban area becomes almost zero for ESL events with a probability of once in 100 years,
 398 even when accounting for SLR up to 2100. Under the most exceptional ESL conditions (RP 250 in 2100), the
 399 barrier is overtopped, generating a flood extent similar to the baseline scenario for the same occurrence
 400 probability.

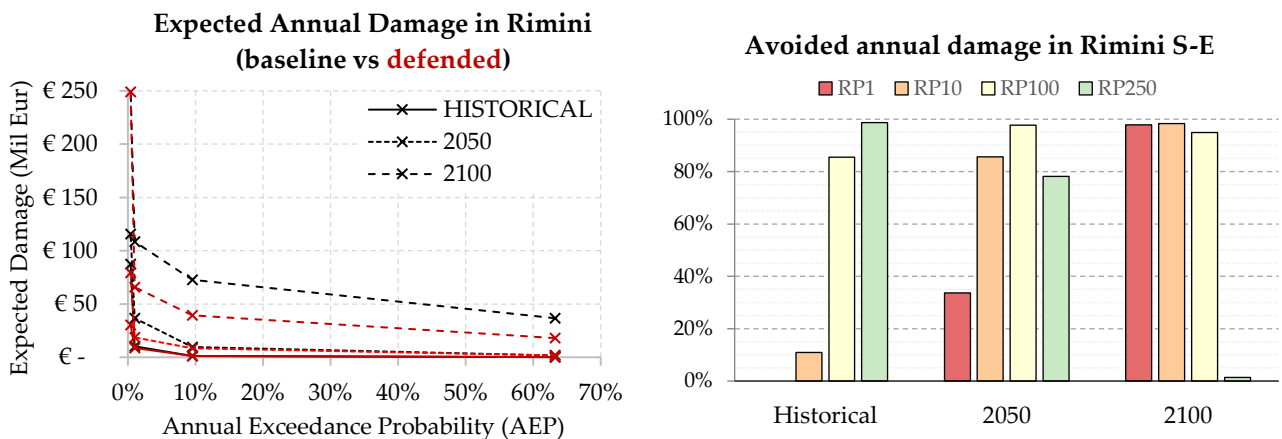


401
 402 **Figure 8.** Cesenatico, extent of land affected by flood according to frequency of occurrence of ESL event up to
 403 2100 for the baseline [left] and the defended scenario [right]. Basemap © Google Maps 2020.

404 In Cesenatico, a barrier designed similarly to *Parco del Mare* could provide significant reduction of flood extents
 405 under most hazard scenarios. Its effectiveness would be greater than in Rimini thanks to the complementary
 406 movable barrier system in use, which seals the port channel allowing to wall off the whole coastal perimeter,
 407 reducing the chance of water ingress in the urban area. In contrast, the erodible winter dune in the baseline
 408 defense scenario can only hold the heavy sea for shorter, less intense ESL events (RP 1 – 10 years), and becomes
 409 ineffective with more exceptional, long-lasting events; from 2050 on, the winter dune could be surmounted
 410 and dismantled by sea waves even during non-exceptional events (RP 1 year).

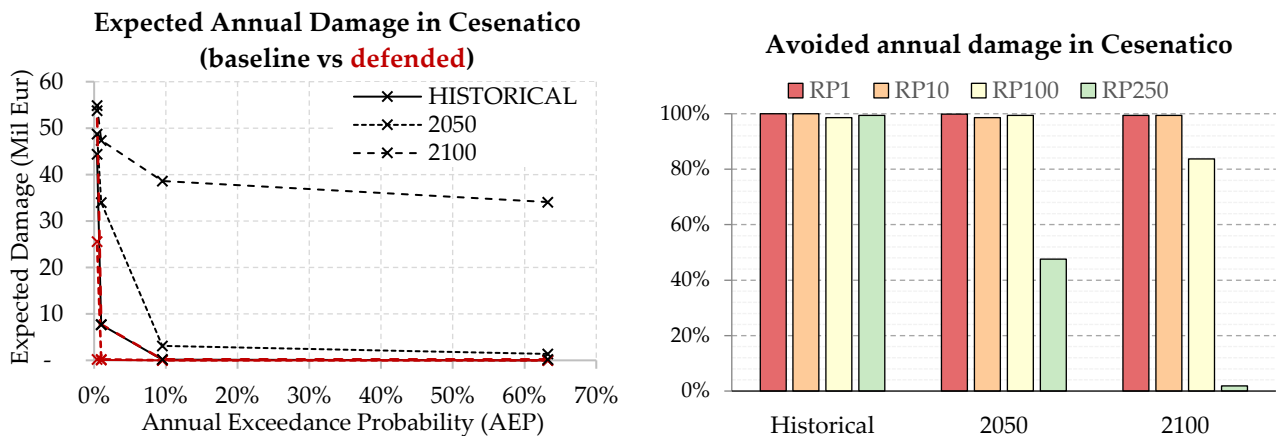
411 **4.2 Expected Annual Damage**

412 The Expected Annual Damage is calculated as a function of maximum exposed value and water depth. In
 413 Rimini, the EAD grows from around 650 thousand Eur under historical conditions to 2.8 million Eur in 2050
 414 and more than 32.3 million Eur in 2100. Under less severe ESL scenarios (RP below 100 years), the risk remains
 415 mostly confined around the marina, which is located outside the defended area, producing an expected
 416 damage below 10 thousand Eur. Under more extreme ESL scenarios, the benefits of the *Parco del Mare* project
 417 protecting the southern part of Rimini become more evident, avoiding about 65% of the expected damages in
 418 the defended scenarios compared to the undefended ones. The damage avoided in the defended scenarios
 419 grow almost linearly with the increase of the baseline EAD under future projections of sea level rise: under
 420 the defended scenario, the EAD is reduced on average by 45% in comparison with the undefended scenario
 421 (Figure 10, left). The project produces benefit up to scenario RP 250 years in 2100, where a projected TWL of
 422 3.5 meters would cause the overtopping of the barrier, reducing the benefits to almost zero (Figure 9, right).



423
 424 **Figure 9.** Rimini: Expected Annual Damage (EAD) according to undefended scenario up to 2100, all town
 425 considered [left]; EAD reduction in the south-eastern part of the town thanks to hazard mitigation offered by
 426 the coastal barrier [right].

427 In Cesenatico, the average EAD for the undefended scenario grows from around 270 thousand Eur under
 428 historical conditions, to 1.7 million Eur in 2050 and almost 26 million Eur in 2100. In our simulations, the
 429 designed defence structure (a static barrier with height of 2.8 m along 7.8 km of coast) is able to avoid most of
 430 the damage inflicted to residential buildings (Figure 11, left). The measure becomes less efficient for the most
 431 extreme scenarios in 2050 and 2100, when the increase in TWL causes the surmounting of the barrier (Figure
 432 10, right). This assessment does not account for the impacts over those beach resorts and bathing facilities
 433 which are located along the barrier or between the barrier and the sea, and thus are equally exposed in both
 434 the baseline and the defended scenario; they would likely represent an additional 7-25% of the baseline
 435 damage.



436
437 **Figure 10.** Cesenatico: Expected Annual Damage (EAD) according to undefended scenario up to 2100 [left];
438 EAD reduction thanks to hazard mitigation offered by the coastal barrier [right].

439 4.3 Cost-Benefit Analysis

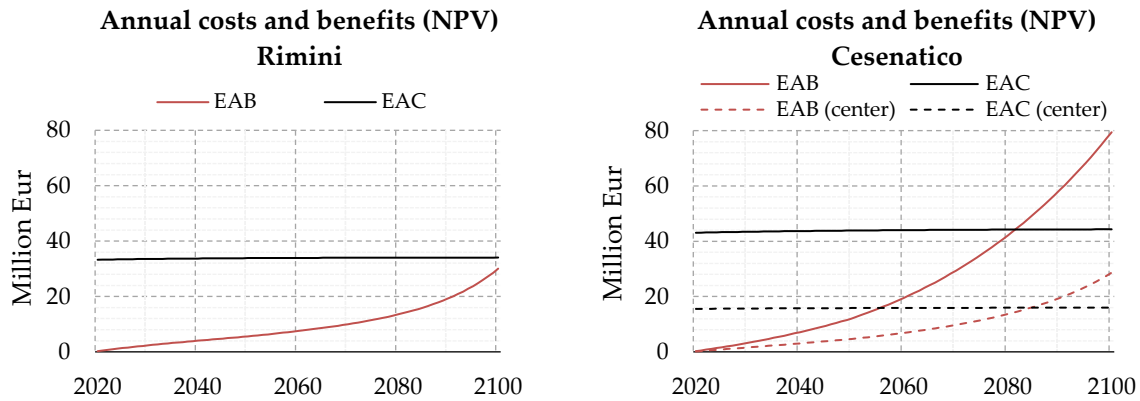
440 The estimates of avoided direct flood impacts are accounted in a DRR-oriented CBA to evaluate the feasibility
441 of mitigation measures in terms of NPV, BCR and payback period for the two time-horizons (2021-2050: 30
442 years; and 2021-2100: 80 years). The assessment does not measure the indirect benefits brought in terms of
443 urban renovation, which are the primary focus of the *Parco del Mare* project, measuring, instead, only the direct
444 benefits in terms of direct flood damage reduction. In Figure 12, the Expected Annual Benefits (EAB) brought
445 by defence measures grow at faster rate approaching 2100 in both sites, because of the larger expected damages
446 from increasing floods severity. The cost of defence implementation is repaid by avoided damage after about
447 40 years in Cesenatico and after 90 years in Rimini. At 2100, the BCR is 0.9 for Rimini and 1.8 for Cesenatico.
448 These results clearly indicate an overall profitability of the defence structure implementation over the long
449 term for Cesenatico. For the case of the municipality of Rimini, further investigation is required in order to
450 account for the non-DRR benefits of the seafront renovation project. For instance, the potential reduction in
451 indirect losses in terms of capital and labour productivity due to less frequent and less intense flooding events,
452 and the potential increase in tourism and well-being of citizens due to renewed urban landscape, are factors
453 that could be accounted for in a holistic CBA analysis and would likely return a shorter payback period.

454 **Table 2.** Summary of CBA for planned or designed seaside defence project in Rimini (all town / south section
455 only) and Cesenatico (all town / center only) over a time horizon of 30 and 80 years (2021 to 2050 and 2021 to
456 2100).

Metrics	Rimini				Cesenatico			
	All town		South only		All town		Center only	
	2050	2100	2050	2100	2050	2100	2050	2100
Baseline EAD [M EUR]	2.8	32	0.5	14.6	1.7	25.9	0.5	12.4
Defended EAD [M EUR]	2.4	17	0.1	0.9	0.1	0.4	0.1	0.4
Expected Annual Benefits [M EUR]	0.3	15	0.4	13.7	1.6	25.5	0.4	11.9
Sum of EAB (discounted) [M EUR]	5.6	30	4.1	27.8	12.0	79.4	4.7	28.6
Sum of EAC (discounted) [M EUR]	33.8	34.0	33.8	34.0	43.8	44.3	15.8	16.0
Net Present Value [M EUR]	-28.3	-4.0	-29.8	-6.3	-31.8	35.1	-11.24	12.6
Benefit-Cost ratio [-]	0.16	0.88	0.12	0.81	0.28	1.79	0.30	1.79

457 In order to better understand the potential benefits of the mitigation measures over different areas of the two
458 municipalities, we compare the results in terms of CBR over a selection of exposed records corresponding to
459 the town higher-density area (i.e. Cesenatico historical center). Table 2 summarizes the metrics of the
460 assessment for different area extent selections. CBA results do not differ much when considering different

461 extents. In Cesenatico benefits grow proportionally to costs, so that the payback time does not change when
 462 considering a section of the town or the whole coastal perimeter.



463
 464 **Figure 11.** Cumulated flood defence costs and expected benefits at Net Present Value for Rimini (left) and
 465 Cesenatico (right).

466 **5. Conclusion**

467 In this study we addressed risk scenarios from coastal inundation over two coastal towns located along the
 468 North Adriatic coastal plain of Italy. This area is projected to become increasingly exposed to ESL events due
 469 to changes in MSL induced by SLR and local subsidence phenomena. Both locations are expected to suffer
 470 increasing economic losses from these events, unless effective coastal adaptation measures are put in place. In
 471 order to understand the upcoming impacts and the potential benefits of designed coastal projects, first we
 472 designed probabilistic ESL scenarios based on local historical observations; then, we projected these scenarios
 473 to 2050 and 2100, accounting for the combined effect of SLR and subsidence rates on the MSL. By using a high-
 474 resolution hydrodynamic model, we produced flood hazard maps associated with each ESL scenario under
 475 both the baseline and the “defended” hypothesis. The defended scenarios accounts for the effect of a coastal
 476 barriers based on the design of *Parco del Mare*, an urban renovation project under construction in Rimini. The
 477 same type of defence structure is envisaged along the coastal perimeter of the nearby town of Cesenatico. The
 478 hazard maps were fed to a locally-calibrated damage model in order to calculate the expected annual damage
 479 for both baseline and defended scenarios.

480 We run a CBA comparing expected damage in terms of flood losses over residential buildings, which represent
 481 the largest share of exposed buildings’ footprints (93%). An increase in damage is expected for both urban
 482 areas from 2021 to 2100: in Cesenatico the EAD grows by a factor 96, in Rimini by a factor 49. The results show
 483 that profitability of present project investment grows over time in both locations, due to the increase of
 484 expected damage triggered by intense ESL events: the EAD under the baseline hypothesis is expected to
 485 increase by 3.5-fold in 2050, up to 10-fold in 2100. The benefits brought by the coastal defence project become
 486 much larger in the second half of the century: the EAB grows 6.1-fold in Rimini, 6.5-fold in Cesenatico, from
 487 2050 to 2100. Avoided losses are expected to match the project implementation costs after about 40 years in
 488 Cesenatico and 90 years in Rimini. Benefits are found to increase proportionally to costs; the payback period
 489 in Cesenatico is the same considering either an investment on the protection of the whole town or only part of
 490 it.

491 Further assessments of these renovation projects should look to measure the indirect and spill-over effects
 492 over the local economy brought by the project, possibly accounting also for the intangible benefits and
 493 scenarios of exposure change. The results are calculated in relation to emission scenario RCP 4.5; compared to
 494 RCP 8.5 at 2050, the difference in SLR contribution is negligible (~0.05 m), while at 2100, the difference between

495 the two emission scenarios is larger (around 0.2 m), thus additional scenario analysis is suggested to better
496 address risk by the end of the century. On the hazard modelling side, the particular consideration of combining
497 wave setup and swash into a single wave contribution component can be considered theoretically
498 questionable, as wave setup is defined as the increase of mean sea level at the shore that is caused by the loss
499 of wave momentum in the surf zone, being often referred as to the static component of wave runup. For future
500 works facing a similar challenge, we recommend to account for wave contribution to TWL as individual
501 dynamic (i.e. swash) and static (runup) components.

502 **Data availability**

503 Mattia Amadio, & Arthur H. Essenfelder (2021). Coastal flood inundation scenarios over Cesenatico and
504 Rimini: hazard and risk for Business as Usual and Defended options [Data set]. Hosted by Zenodo:
505 <https://zenodo.org/record/4783443>

506 **Authors contribution**

507 MA, AHE and SB conceptualized the study and designed the experiments. AHE carried out the coastal hazard
508 modelling. SR advised the model setup and calculation. SB and PM provided required data and expertise
509 about the case study areas. MA performed the economic risk modelling and wrote the manuscript. SM
510 supported the CBA calculations. JM and SB managed the funding acquisition and project supervision. All co-
511 authors have reviewed the manuscript.

512 **Acknowledgment**

513 The research leading to this paper received funding through the projects CLARA (EU's Horizon 2020 research
514 and innovation programme under grant agreement 730482), SAFERPLACES (Climate-KIC innovation
515 partnership) and EUCP – European Climate Prediction system under grant agreement 776613. We want to
516 thank Luisa Perini for her kind support.

517 **References**

- 518 Amadio, M., Scorzini, A. R., Carisi, F., Essenfelder, A. H., Domeneghetti, A., Mysiak, J., and Castellarin, A.:
519 Testing empirical and synthetic flood damage models: the case of Italy, *Nat. Hazards Earth Syst. Sci.*, 19,
520 661–678, <https://doi.org/10.5194/nhess-19-661-2019>, 2019.
- 521 Anderson, T. R., Fletcher, C. H., Barbee, M. M., Romine, B. M., Lemmo, S., and Delevaux, J. M. S. M. S.:
522 Modeling multiple sea level rise stresses reveals up to twice the land at risk compared to strictly passive
523 flooding methods, *Sci. Rep.*, 8, 14484, <https://doi.org/10.1038/s41598-018-32658-x>, 2018.
- 524 Annunziato, A. and Probst, P.: Continuous Harmonics Analysis of Sea Level Measurements: Description of a
525 new method to determine sea level measurement tidal component, <https://doi.org/10.2788/4295>, 2016.
- 526 Antonioli, F., Anzidei, M., Amorosi, A., Lo Presti, V., Mastronuzzi, G., Deiana, G., De Falco, G., Fontana, A.,
527 Fontolan, G., Lisco, S., Marsico, A., Moretti, M., Orrù, P. E., Sannino, G. M., Serpelloni, E., and Vecchio, A.:
528 Sea-level rise and potential drowning of the Italian coastal plains: Flooding risk scenarios for 2100, *Quat. Sci.*
529 *Rev.*, 158, 29–43, <https://doi.org/10.1016/j.quascirev.2016.12.021>, 2017.
- 530 Armaroli, C. and Duo, E.: Validation of the coastal storm risk assessment framework along the Emilia-
531 Romagna coast, *Coast. Eng.*, 134, 159–167, <https://doi.org/10.1016/j.coastaleng.2017.08.014>, 2018.
- 532 Armaroli, C., Ciavola, P., Masina, M., and Perini, L.: Run-up computation behind emerged breakwaters for
533 marine storm risk assessment on JSTOR, *J. Coast. Res.*, II, 1612–1616, 2009.
- 534 Armaroli, C., Ciavola, P., Perini, L., Calabrese, L., Lorito, S., Valentini, A., and Masina, M.: Critical storm

535 thresholds for significant morphological changes and damage along the Emilia-Romagna coastline, Italy,
536 143–144, 34–51, <https://doi.org/10.1016/j.geomorph.2011.09.006>, 2012.

537 ARPA Emilia-Romagna: Relazione Tecnica - Mappe della pericolosità e del rischio di alluvioni in ambito
538 costiero, distretto Appennino Settentrionale, [https://ambiente.regione.emilia-romagna.it/it/suolo-](https://ambiente.regione.emilia-romagna.it/it/suolo-bacino/sezioni/piano-di-gestione-del-rischio-alluvioni/piano-gestione-del-rischio-alluvioni/documenti-1/relazioni-tecniche-mappe/relazione-tecnica-mappe-della-pericolosita2019-e-del-rischio-di-alluvioni-)
539 [bacino/sezioni/piano-di-gestione-del-rischio-alluvioni/piano-gestione-del-rischio-alluvioni/documenti-](https://ambiente.regione.emilia-romagna.it/it/suolo-bacino/sezioni/piano-di-gestione-del-rischio-alluvioni/piano-gestione-del-rischio-alluvioni/documenti-1/relazioni-tecniche-mappe/relazione-tecnica-mappe-della-pericolosita2019-e-del-rischio-di-alluvioni-)
540 [1/relazioni-tecniche-mappe/relazione-tecnica-mappe-della-pericolosita2019-e-del-rischio-di-alluvioni-](https://ambiente.regione.emilia-romagna.it/it/suolo-bacino/sezioni/piano-di-gestione-del-rischio-alluvioni/piano-gestione-del-rischio-alluvioni/documenti-1/relazioni-tecniche-mappe/relazione-tecnica-mappe-della-pericolosita2019-e-del-rischio-di-alluvioni-), 2019.

541 Barnard, P. L., Erikson, L. H., Foxgrover, A. C., Hart, J. A. F., Limber, P., O'Neill, A. C., van Ormondt, M.,
542 Vitousek, S., Wood, N., Hayden, M. K., and Jones, J. M.: Dynamic flood modeling essential to assess the
543 coastal impacts of climate change, *Sci. Rep.*, 9, 1–13, <https://doi.org/10.1038/s41598-019-40742-z>, 2019.

544 Bates, P. D., Dawson, R. J., Hall, J. W., Horritt, M. S., Nicholls, R. J., Wicks, J., and Ali Mohamed Hassan, M.
545 A.: Simplified two-dimensional numerical modelling of coastal flooding and example applications, *Coast.*
546 *Eng.*, 52, 793–810, <https://doi.org/10.1016/j.coastaleng.2005.06.001>, 2005.

547 Boardman, A. E., Greenberg, D. H., Vining, A. R., and Weimer, D. L.: *Cost-Benefit Analysis*, Cambridge
548 University Press, <https://doi.org/10.1017/9781108235594>, 2018.

549 Bonaduce, A., Pinardi, N., Oddo, P., Spada, G., and Larnicol, G.: Sea-level variability in the Mediterranean
550 Sea from altimetry and tide gauges, *Clim. Dyn.*, 47, 2851–2866, <https://doi.org/10.1007/s00382-016-3001-2>,
551 2016.

552 Boon, J. D.: *Secrets of the Tide*, Elsevier, 1–210 pp., <https://doi.org/10.1016/C2013-0-18114-7>, 2011.

553 Bos, F. and Zwaneveld, P.: Cost-Benefit Analysis for Flood Risk Management and Water Governance in the
554 Netherlands: An Overview of One Century, *SSRN Electron. J.*, <https://doi.org/10.2139/ssrn.3023983>, 2017.

555 Bouwer, L. M.: Have disaster losses increased due to anthropogenic climate change?, *Bull. Am. Meteorol.*
556 *Soc.*, <https://doi.org/10.1175/2010BAMS3092.1>, 2011.

557 Breilh, J. F., Chaumillon, E., Bertin, X., and Gravelle, M.: Assessment of static flood modeling techniques:
558 Application to contrasting marshes flooded during Xynthia (western France), *Nat. Hazards Earth Syst. Sci.*,
559 13, 1595–1612, <https://doi.org/10.5194/nhess-13-1595-2013>, 2013.

560 Carbognin, L., Teatini, P., and Tosi, L.: The impact of relative sea level rise on the Northern Adriatic Sea
561 coast, Italy, in: *WIT Transactions on Ecology and the Environment*, 137–148,
562 <https://doi.org/10.2495/RAV090121>, 2009.

563 Carbognin, L., Teatini, P., Tomasin, A., and Tosi, L.: Global change and relative sea level rise at Venice: What
564 impact in term of flooding, *Clim. Dyn.*, 35, 1055–1063, <https://doi.org/10.1007/s00382-009-0617-5>, 2010.

565 Carminati, E. and Martinelli, G.: Subsidence rates in the Po Plain, northern Italy: the relative impact of
566 natural and anthropogenic causation, *Eng. Geol.*, 66, 241–255, [https://doi.org/10.1016/S0013-7952\(02\)00031-5](https://doi.org/10.1016/S0013-7952(02)00031-5),
567 2002.

568 Church, J. A. and White, N. J.: Sea-Level Rise from the Late 19th to the Early 21st Century, *Surv. Geophys.*,
569 32, 585–602, <https://doi.org/10.1007/s10712-011-9119-1>, 2011.

570 Ciavola, P. and Coco, G. (Eds.): *Coastal storms: processes and impacts*, Wiley-Blackwell, 266 pp., 2017.

571 Comune di Rimini: Parco del Mare Sud - Strategia per la rigenerazione urbana, <https://bit.ly/3kwNoB1>, 2018.

572 Comune di Rimini: Deliberazione originale di giunta comunale N. 118 del 02/05/2019,
573 https://www.comune.rimini.it/sites/default/files/2021-06/dlg_00118_02-05-2019.pdf, 2019a.

574 Comune di Rimini: Deliberazione originale di giunta comunale N. 99 del 11/04/2019,
575 https://www.comune.rimini.it/sites/default/files/2021-06/dlg_00099_11-04-2019_0.pdf, 2019b.

576 Comune di Rimini: Deliberazione originale di giunta comunale N. 128 del 26/05/2020,
577 https://www.comune.rimini.it/sites/default/files/2021-06/dlg_00128_26-05-2020.pdf, 2020.

578 Comune di Rimini: Deliberazione originale di giunta comunale N. 19 del 19/01/2021,
579 https://www.comune.rimini.it/sites/default/files/2021-06/dlg_00019_19-01-2021.pdf, 2021a.

580 Comune di Rimini: Deliberazione originale di giunta comunale N. 20 del 19/01/2021,
581 https://www.comune.rimini.it/sites/default/files/2021-06/dlg_00020_19-01-2021.pdf, 2021b.

582 CRESME: I costi di costruzione in edilizia residenziale, industriale per uffici ed alberghiera,
583 <http://cresme.cineas.it>, 2019.

584 Dottori, F., Martina, M. L. V., and Figueiredo, R.: A methodology for flood susceptibility and vulnerability
585 analysis in complex flood scenarios, *J. Flood Risk Manag.*, 11, S632–S645, <https://doi.org/10.1111/jfr3.12234>,
586 2018.

587 Familkhalili, R., Talke, S. A., and Jay, D. A.: Tide-Storm Surge Interactions in Highly Altered Estuaries: How
588 Channel Deepening Increases Surge Vulnerability, *J. Geophys. Res. Ocean.*, 125, e2019JC015286,
589 <https://doi.org/10.1029/2019JC015286>, 2020.

590 Fuhrmann, C. M., Wood, K. M., and Rodgers, J. C.: Assessment of storm surge and structural damage on San
591 Salvador Island, Bahamas, associated with Hurricane Joaquin (2015), *Nat. Hazards*, 99, 913–930,
592 <https://doi.org/10.1007/s11069-019-03782-2>, 2019.

593 Gambolati, G., Giunta, G., Putti, M., Teatini, P., Tomasi, L., Betti, I., and Morelli, M.: Coastal Evolution of the
594 Upper Adriatic Sea due to Sea Level Rise and Natural and Anthropogenic Land Subsidence, 1–34,
595 <https://doi.org/10.1007/978-94-011-5147-4>, 1998.

596 Garnier, E., Ciavola, P., Spencer, T., Ferreira, O., Armaroli, C., and McIvor, A.: Historical analysis of storm
597 events: Case studies in France, England, Portugal and Italy, *Coast. Eng.*, 134, 10–23,
598 <https://doi.org/10.1016/j.coastaleng.2017.06.014>, 2018.

599 Hallegatte, S., Green, C., Nicholls, R. J., and Corfee-Morlot, J.: Future flood losses in major coastal cities, *Nat.*
600 *Clim. Chang.*, <https://doi.org/10.1038/nclimate1979>, 2013.

601 Hinkel, J., Nicholls, R. J., Vafeidis, A. T., Tol, R. S. J., and Avagianou, T.: Assessing risk of and adaptation to
602 sea-level rise in the European Union: An application of DIVA, *Mitig. Adapt. Strateg. Glob. Chang.*,
603 <https://doi.org/10.1007/s11027-010-9237-y>, 2010.

604 Hinkel, J., Lincke, D., Vafeidis, A. T., Perrette, M., Nicholls, R. J., Tol, R. S. J., Marzeion, B., Fettweis, X.,
605 Ionescu, C., and Levermann, A.: Coastal flood damage and adaptation costs under 21st century sea-level
606 rise, *Proc. Natl. Acad. Sci.*, 111, 3292–3297, <https://doi.org/10.1073/pnas.1222469111>, 2014.

607 Huizinga, J., Moel, H. De, and Szewczyk, W.: Global flood depth-damage functions : Methodology and the
608 Database with Guidelines, 1–108 pp., <https://doi.org/10.2760/16510>, 2017.

609 Idier, D., Bertin, X., Thompson, P., and Pickering, M. D.: Interactions Between Mean Sea Level, Tide, Surge,
610 Waves and Flooding: Mechanisms and Contributions to Sea Level Variations at the Coast,
611 <https://doi.org/10.1007/s10712-019-09549-5>, 1 November 2019.

612 ISPRA: Mare e ambiente costiero, Tematiche in Primo Piano - Annuario dei dati ambientali 2011, 259–322
613 pp., <https://www.isprambiente.gov.it/it/pubblicazioni/stato-dellambiente/tematiche-in-primo-piano-annuario-dei-dati-ambientali-2011>, 2012.

614 Rete Mareografica Nazionale:
615 <https://www.mareografico.it/?session=0S2731884245M826885M79QA&syslng=ita&systemen=-1&sysind=-1&sysub=-1&sysfnt=0&code=STAZ&idst=15>, last access: 19 October 2021.

616
617
618 15° censimento della popolazione e delle abitazioni: <http://dati-censimentopopolazione.istat.it>, last access: 1
619 April 2019.

620 Jongman, B., Kreibich, H., Apel, H., Barredo, J. I., Bates, P. D., Feyen, L., Gericke, A., Neal, J., Aerts, J. C. J. H.,
621 and Ward, P. J.: Comparative flood damage model assessment: towards a European approach, *Nat. Hazards*
622 *Earth Syst. Sci.*, 12, 3733–3752, 2012a.

623 Jongman, B., Ward, P. J., and Aerts, J. C. J. H.: Global exposure to river and coastal flooding: Long term
624 trends and changes, *Glob. Environ. Chang.*, <https://doi.org/10.1016/j.gloenvcha.2012.07.004>, 2012b.

625 Jonkman, S. N., Brinkhuis-Jak, M., and Kok, M.: Cost benefit analysis and flood damage mitigation in the
626 Netherlands, 49, 95–111, 2004.

627 Kain, C. L., Lewarn, B., Rigby, E. H., and Mazengarb, C.: Tsunami Inundation and Maritime Hazard
628 Modelling for a Maximum Credible Tsunami Scenario in Southeast Tasmania, Australia, *Pure Appl.*
629 *Geophys.*, 177, 1549–1568, <https://doi.org/10.1007/s00024-019-02384-0>, 2020.

630 Kemp, A. C., Horton, B. P., Donnelly, J. P., Mann, M. E., Vermeer, M., and Rahmstorf, S.: Climate related sea-
631 level variations over the past two millennia, *Proc. Natl. Acad. Sci.*, 108, 11017–11022,
632 <https://doi.org/10.1073/pnas.1015619108>, 2011.

633 Kind, J. M.: Economically efficient flood protection standards for the Netherlands, *J. Flood Risk Manag.*, 7,
634 103–117, <https://doi.org/10.1111/jfr3.12026>, 2014.

635 Kirezci, E., Young, I. R., Ranasinghe, R., Muis, S., Nicholls, R. J., Lincke, D., and Hinkel, J.: Projections of
636 global-scale extreme sea levels and resulting episodic coastal flooding over the 21st Century, *Sci. Rep.*, 10,
637 11629, <https://doi.org/10.1038/s41598-020-67736-6>, 2020.

638 Kumbier, K., Carvalho, R. C., Vafeidis, A. T., and Woodroffe, C. D.: Comparing static and dynamic flood
639 models in estuarine environments: a case study from south-east Australia, *Mar. Freshw. Res.*, 70, 781,
640 <https://doi.org/10.1071/MF18239>, 2019.

641 Lambeck, K. and Purcell, A.: Sea-level change in the Mediterranean Sea since the LGM: model predictions
642 for tectonically stable areas, *Quat. Sci. Rev.*, 24, 1969–1988, <https://doi.org/10.1016/j.quascirev.2004.06.025>,
643 2005.

644 Lambeck, K., Antonioli, F., Anzidei, M., Ferranti, L., Leoni, G., Scicchitano, G., and Silenzi, S.: Sea level
645 change along the Italian coast during the Holocene and projections for the future, *Quat. Int.*, 232, 250–257,
646 <https://doi.org/10.1016/j.quaint.2010.04.026>, 2011.

647 Lewis, M., Bates, P., Horsburgh, K., Neal, J., and Schumann, G.: A storm surge inundation model of the
648 northern Bay of Bengal using publicly available data, *Q. J. R. Meteorol. Soc.*, 139, 358–369,
649 <https://doi.org/10.1002/qj.2040>, 2013.

650 Li, M., Zhang, F., Barnes, S., and Wang, X.: Assessing storm surge impacts on coastal inundation due to
651 climate change: case studies of Baltimore and Dorchester County in Maryland, *Nat. Hazards*, 103, 2561–2588,
652 <https://doi.org/10.1007/s11069-020-04096-4>, 2020.

653 Lionello, P.: The climate of the Venetian and North Adriatic region: Variability, trends and future change,
654 *Phys. Chem. Earth, Parts A/B/C*, 40–41, 1–8, <https://doi.org/10.1016/j.pce.2012.02.002>, 2012.

655 Lionello, P., Conte, D., Marzo, L., and Scarascia, L.: The contrasting effect of increasing mean sea level and
656 decreasing storminess on the maximum water level during storms along the coast of the Mediterranean Sea
657 in the mid 21st century, *Glob. Planet. Change*, 151, 80–91, <https://doi.org/10.1016/j.gloplacha.2016.06.012>,
658 2017.

659 Lionello, P., Barriopedro, D., Ferrarin, C., Nicholls, R., Orlic, M., Raicich, F., Reale, M., Umgiesser, G.,
660 Vousdoukas, M., and Zanchettin, D.: Extremes floods of Venice: characteristics, dynamics, past and future
661 evolution, *Nat. Hazards Earth Syst. Sci.*, 1–34, <https://doi.org/10.5194/nhess-2020-359>, 2020.

662 Lionello, P., Barriopedro, D., Ferrarin, C., Nicholls, R. J., Orlić, M., Raicich, F., Reale, M., Umgiesser, G.,
663 Vousdoukas, M., and Zanchettin, D.: Extreme floods of Venice: Characteristics, dynamics, past and future
664 evolution (review article), <https://doi.org/10.5194/nhess-21-2705-2021>, 1 September 2021.

665 Lowe, J.: Intergenerational wealth transfers and social discounting: Supplementary Green Book guidance,
666 HM Treasury, London, 3–6, 2008.

667 Lowe, J., Gregory, J., and Flather, R.: Changes in the occurrence of storm surges around the United Kingdom
668 under a future climate scenario using a dynamic storm surge model driven by the Hadley Centre climate
669 models, *Clim. Dyn.*, 18, 179–188, 2001.

670 Marsico, A., Lisco, S., Lo Presti, V., Antonioli, F., Amorosi, A., Anzidei, M., Deiana, G., De Falco, G., Fontana,
671 A., Fontolan, G., Moretti, M., Orrú, P. E., Serpelloni, E., Sannino, G., Vecchio, A., and Mastronuzzi, G.:
672 Flooding scenario for four Italian coastal plains using three relative sea level rise models, *J. Maps*, 13, 961–
673 967, <https://doi.org/10.1080/17445647.2017.1415989>, 2017.

674 Masina, M., Lamberti, A., and Archetti, R.: Coastal flooding: A copula based approach for estimating the
675 joint probability of water levels and waves, *Coast. Eng.*, 97, 37–52,
676 <https://doi.org/10.1016/j.coastaleng.2014.12.010>, 2015.

677 McGranahan, G., Balk, D., and Anderson, B.: The rising tide: Assessing the risks of climate change and

678 human settlements in low elevation coastal zones, *Environ. Urban,*
679 <https://doi.org/10.1177/0956247807076960>, 2007.

680 McInnes, K. L., Walsh, K. J. E., Hubbert, G. D., and Beer, T.: Impact of sea-level rise and storm surges in a
681 coastal community, *Nat. Hazards*, 30, 187–207, <https://doi.org/10.1023/A:1026118417752>, 2003.

682 McInnes, K. L., O’Grady, J. G., and Hubbert, G. D.: Modelling sea level extremes from storm surges and
683 wave setup for climate change assessments in Southeastern Australia, in: *Journal of Coastal Research*, 1005–
684 1009, 2009.

685 Mechler, R.: Reviewing estimates of the economic efficiency of disaster risk management: opportunities and
686 limitations of using risk-based cost–benefit analysis, *Nat. Hazards*, 81, 2121–2147,
687 <https://doi.org/10.1007/s11069-016-2170-y>, 2016.

688 Melet, A., Almar, R., Hemer, M., Le Cozannet, G., Meyssignac, B., and Ruggiero, P.: Contribution of Wave
689 Setup to Projected Coastal Sea Level Changes, *J. Geophys. Res. Ocean.*, 125, e2020JC016078,
690 <https://doi.org/10.1029/2020JC016078>, 2020.

691 Meli, M., Olivieri, M., and Romagnoli, C.: Sea-Level Change along the Emilia-Romagna Coast from Tide
692 Gauge and Satellite Altimetry, *Remote Sens.*, 13, 97, <https://doi.org/10.3390/rs13010097>, 2020.

693 Meyssignac, B. and Cazenave, A.: Sea level: A review of present-day and recent-past changes and variability,
694 *J. Geodyn.*, 58, 96–109, <https://doi.org/10.1016/j.jog.2012.03.005>, 2012.

695 Mitchum, G. T., Nerem, R. S., Merrifield, M. A., and Gehrels, W. R.: Modern Sea-Level-Change Estimates, in:
696 *Understanding Sea-Level Rise and Variability*, Wiley-Blackwell, Oxford, UK, UK, 122–142,
697 <https://doi.org/10.1002/9781444323276.ch5>, 2010.

698 Muis, S., Güneralp, B., Jongman, B., Aerts, J. C. J. H., and Ward, P. J.: Flood risk and adaptation strategies
699 under climate change and urban expansion: A probabilistic analysis using global data, *Sci. Total Environ.*,
700 538, 445–457, <https://doi.org/10.1016/j.scitotenv.2015.08.068>, 2015.

701 Muis, S., Verlaan, M., Winsemius, H. C., Aerts, J. C. J. H., and Ward, P. J.: A global reanalysis of storm surges
702 and extreme sea levels, *Nat. Commun.*, 7, 11969, <https://doi.org/10.1038/ncomms11969>, 2016.

703 Muis, S., Apecechea, M. I., Dullaart, J., de Lima Rego, J., Madsen, K. S., Su, J., Yan, K., and Verlaan, M.: A
704 High-Resolution Global Dataset of Extreme Sea Levels, Tides, and Storm Surges, Including Future
705 Projections, *Front. Mar. Sci.*, 7, 263, <https://doi.org/10.3389/fmars.2020.00263>, 2020.

706 Nicholls, R. J. and Cazenave, A.: Sea-Level Rise and Its Impact on Coastal Zones, *Science (80-.)*, 328, 1517–
707 1520, <https://doi.org/10.1126/science.1185782>, 2010.

708 Olsen, A. S., Zhou, Q., Linde, J. J., and Arnbjerg-Nielsen, K.: Comparing methods of calculating expected
709 annual damage in urban pluvial flood risk assessments, 7, 255–270, <https://doi.org/10.3390/w7010255>, 2015.

710 Open Street Map data for Nord-Est Italy: <http://download.geofabrik.de/europe/italy/nord-est.html>, last
711 access: 1 April 2019.

712 Peltier, W. R.: Global glacial isostasy and the surface of the ice-age Earth: the ICE-5G model and GRACE,
713 *Annu. Rev. Earth Planet. Sci.*, 32, 111–149, <https://doi.org/10.1146/annurev.earth.32.082503.144359>, 2004.

714 Peltier, W. R., Argus, D. F., and Drummond, R.: Space geodesy constrains ice age terminal deglaciation: The
715 global ICE-6G_C (VM5a) model, *J. Geophys. Res. Solid Earth*, 120, 450–487,
716 <https://doi.org/10.1002/2014JB011176>, 2015.

717 Perini, L., Calabrese, L., Deserti, M., Valentini, A., Ciavola, P., and Armaroli, C.: Le mareggiate e gli impatti
718 sulla costa in Emilia-Romagna 1946-2010, *Quaderni ARPA*,
719 https://www.researchgate.net/publication/290441941_Le_mareggiate_e_gli_impatti_sulla_costa_in_Emilια-Romagna_1946-2010, 2011.

721 Perini, L., Calabrese, L., Salerno, G., and Luciani, P.: Mapping of flood risk in Emilia-Romagna coastal areas,
722 in: *LXXXVI Congresso della Società Geologica Italiana*, 501–502,
723 <https://doi.org/http://dx.doi.org/10.13140/2.1.1703.7766>, 2012.

724 Perini, L., Calabrese, L., Lorito, S., and Luciani, P.: Il rischio da mareggiata in Emilia-Romagna: l’evento del
725 5-6 Febbraio 2015, *il Geologo*, 8–17 pp., <http://www.geologiemiariomagna.it/wp->

726 content/uploads/Art_Costa.pdf, 2015.

727 Perini, L., Calabrese, L., Salerno, G., Ciavola, P., and Armaroli, C.: Evaluation of coastal vulnerability to
728 flooding: comparison of two different methodologies adopted by the Emilia-Romagna region (Italy), *Nat.*
729 *Hazards Earth Syst. Sci.*, 16, 181–194, <https://doi.org/10.5194/nhess-16-181-2016>, 2016.

730 Perini, L., Calabrese, L., Luciani, P., Olivieri, M., Galassi, G., and Spada, G.: Sea-level rise along the Emilia-
731 Romagna coast (Northern Italy) in 2100: scenarios and impacts, *Nat. Hazards Earth Syst. Sci.*, 17, 2271–2287,
732 <https://doi.org/10.5194/nhess-17-2271-2017>, 2017.

733 Polcari, M., Albano, M., Montuori, A., Bignami, C., Tolomei, C., Pezzo, G., Falcone, S., Piana, C. La, Doumaz,
734 F., Salvi, S., and Stramondo, S.: InSAR monitoring of Italian coastline revealing natural and anthropogenic
735 ground deformation phenomena and future perspectives, *Sustain.*, 10, 4–7,
736 <https://doi.org/10.3390/su10093152>, 2018.

737 Pörtner, H. O., Roberts, D. C., Masson-Delmotte, V., Zhai, P., Tignor, M., Poloczanska, E., Mintenbeck, K.,
738 Alegría, A., Nicolai, M., Okem, A., Petzold, J., Rama, B., and Weyer, N. M.: IPCC Special Report on the
739 Ocean and Cryosphere in a Changing Climate, IPCC, <https://www.ipcc.ch/srocc>, 2019.

740 Price, R.: Cost-effectiveness of disaster risk reduction and adaptation to climate change, 1–21, 2018.

741 Ramirez, J. A., Lichter, M., Coulthard, T. J., and Skinner, C.: Hyper-resolution mapping of regional storm
742 surge and tide flooding: comparison of static and dynamic models, *Nat. Hazards*, 82, 571–590,
743 <https://doi.org/10.1007/s11069-016-2198-z>, 2016.

744 Roberts, S.: ANUGA - Open source hydrodynamic/hydraulic modelling, <https://anuga.anu.edu.au>, 2020.

745 Roberts, S., Nielsen, O., Gray, D., and Sexton, J.: ANUGA User Manual,
746 <https://doi.org/10.13140/RG.2.2.12401.99686>, 2015.

747 Scarascia, L. and Lionello, P.: Global and regional factors contributing to the past and future sea level rise in
748 the Northern Adriatic Sea, *Glob. Planet. Change*, 106, 51–63, <https://doi.org/10.1016/j.gloplacha.2013.03.004>,
749 2013.

750 Seenath, A., Wilson, M., and Miller, K.: Hydrodynamic versus GIS modelling for coastal flood vulnerability
751 assessment: Which is better for guiding coastal management?, *Ocean Coast. Manag.*, 120, 99–109,
752 <https://doi.org/10.1016/j.ocecoaman.2015.11.019>, 2016.

753 Skinner, C. J., Coulthard, T. J., Parsons, D. R., Ramirez, J. A., Mullen, L., and Manson, S.: Simulating tidal and
754 storm surge hydraulics with a simple 2D inertia based model, in the Humber Estuary, U.K, *Estuar. Coast.*
755 *Shelf Sci.*, 155, 126–136, <https://doi.org/10.1016/j.ecss.2015.01.019>, 2015.

756 Smith, R. A. E., Bates, P. D., and Hayes, C.: Evaluation of a coastal flood inundation model using hard and
757 soft data, *Environ. Model. Softw.*, 30, 35–46, <https://doi.org/10.1016/j.envsoft.2011.11.008>, 2012.

758 Solari, L., Del Soldato, M., Bianchini, S., Ciampalini, A., Ezquerro, P., Montalti, R., Raspini, F., and Moretti,
759 S.: From ERS 1/2 to Sentinel-1: Subsidence Monitoring in Italy in the Last Two Decades, *Front. Earth Sci.*, 6,
760 <https://doi.org/10.3389/feart.2018.00149>, 2018.

761 Stocker, T. F., Dahe, Q., Plattner, G.-K., Alexander, L. V., Allen, S. K., Bindoff, N. L., Bréon, F.-M., Church, J.
762 A., Cubash, U., Emori, S., Forster, P., Friedlingstein, P., Talley, L. D., Vaughan, D. G., and Xie, S.-P.: Technical
763 Summary, in: *Climate Change 2013: The Physical Science Basis. Contribution of Working Group I to the Fifth*
764 *Assessment Report of the Intergovernmental Panel on Climate Change*, edited by: Stocker, T. F., Qin, D.,
765 Plattner, G.-K., Tignor, M., Allen, S. K., Boschung, J., Nauels, A., Y. Xia, V. B., and Midgley, P. M., Cambridge
766 University Press, Cambridge, United Kingdom and New York, NY, USA., 33–115, [https://doi.org/10.1017/](https://doi.org/10.1017/CBO9781107415324.005)
767 [CBO9781107415324.005](https://doi.org/10.1017/CBO9781107415324.005), 2013.

768 Syvitski, J. P. M., Kettner, A. J., Overeem, I., Hutton, E. W. H., Hannon, M. T., Brakenridge, G. R., Day, J.,
769 Vörösmarty, C., Saito, Y., Giosan, L., and Nicholls, R. J.: Sinking deltas due to human activities, *Nat. Geosci.*,
770 <https://doi.org/10.1038/ngeo629>, 2009.

771 Teatini, P., Ferronato, M., Gambolati, G., Bertoni, W., and Gonella, M.: A century of land subsidence in
772 Ravenna, Italy, *Environ. Geol.*, 47, 831–846, <https://doi.org/10.1007/s00254-004-1215-9>, 2005.

773 Teatini, P., Ferronato, M., Gambolati, G., and Gonella, M.: Groundwater pumping and land subsidence in

774 the Emilia-Romagna coastland, Italy: Modeling the past occurrence and the future trend, *Water Resour. Res.*,
775 42, <https://doi.org/10.1029/2005WR004242>, 2006.

776 Teng, J., Jakeman, A. J., Vaze, J., Croke, B. F. W., Dutta, D., and Kim, S.: Flood inundation modelling: A
777 review of methods, recent advances and uncertainty analysis, <https://doi.org/10.1016/j.envsoft.2017.01.006>, 1
778 April 2017.

779 Tsimplis, M. N. and Rixen, M.: Sea level in the Mediterranean Sea: The contribution of temperature and
780 salinity changes, *Geophys. Res. Lett.*, 29, 51-1-51-4, <https://doi.org/10.1029/2002gl015870>, 2002.

781 Tsimplis, M. N., Marcos, M., and Somot, S.: 21st century Mediterranean sea level rise: Steric and atmospheric
782 pressure contributions from a regional model, *Glob. Planet. Change*, 63, 105–111,
783 <https://doi.org/10.1016/j.gloplacha.2007.09.006>, 2008.

784 Tsimplis, M. N., Raicich, F., Fenoglio-Marc, L., Shaw, A. G. P., Marcos, M., Somot, S., and Bergamasco, A.:
785 Recent developments in understanding sea level rise at the Adriatic coasts, *Phys. Chem. Earth*, 40–41, 59–71,
786 <https://doi.org/10.1016/j.pce.2009.11.007>, 2012.

787 Umgiesser, G., Bajo, M., Ferrarin, C., Cucco, A., Lionello, P., Zanchettin, D., Papa, A., Tosoni, A., Ferla, M.,
788 Coraci, E., Morucci, S., Crosato, F., Bonometto, A., Valentini, A., Orlic, M., Haigh, I., Nielsen, J. W., Bertin, X.,
789 Fortunato, A. B., Pérez Gómez, B., Alvarez Fanjul, E., Paradis, D., Jourdan, D., Pasquet, A., Mourre, B.,
790 Tintoré, J., and Nicholls, R.: The prediction of floods in Venice: methods, models and uncertainty, *Nat.*
791 *Hazards Earth Syst. Sci.*, 1–47, <https://doi.org/10.5194/nhess-2020-361>, 2020.

792 Vousdoukas, M. I., Voukouvalas, E., Mentaschi, L., Dottori, F., Giardino, A., Bouziotas, D., Bianchi, A.,
793 Salamon, P., and Feyen, L.: Developments in large-scale coastal flood hazard mapping, *Nat. Hazards Earth*
794 *Syst. Sci.*, 16, 1841–1853, <https://doi.org/10.5194/nhess-16-1841-2016>, 2016.

795 Vousdoukas, M. I., Mentaschi, L., Feyen, L., and Voukouvalas, E.: Extreme sea levels on the rise along
796 Europe’s coasts, *Earth’s Futur.*, 5, 1–20, <https://doi.org/10.1002/ef2.192>, 2017.

797 Vousdoukas, M. I., Mentaschi, L., Voukouvalas, E., Verlaan, M., Jevrejeva, S., Jackson, L. P., and Feyen, L.:
798 Global probabilistic projections of extreme sea levels show intensification of coastal flood hazard, *Nat.*
799 *Commun.*, 9, 1–12, <https://doi.org/10.1038/s41467-018-04692-w>, 2018.

800 Wang, S., Najafi, M. R., Cannon, A. J., and Khan, A. A.: Uncertainties in Riverine and Coastal Flood Impacts
801 under Climate Change, 13, 1774, <https://doi.org/10.3390/w13131774>, 2021.

802 Wöppelmann, G. and Marcos, M.: Coastal sea level rise in southern Europe and the nonclimate contribution
803 of vertical land motion, *J. Geophys. Res. Ocean.*, 117, <https://doi.org/10.1029/2011JC007469>, 2012.

804 Zanchettin, D., Traverso, P., and Tomasino, M.: Observations on future sea level changes in the Venice
805 lagoon, *Hydrobiologia*, <https://doi.org/10.1007/s10750-006-0416-5>, 2007.

806 Zanchettin, D., Bruni, S., Raicich, F., Lionello, P., Adloff, F., Androsov, A., Antonioli, F., Artale, V.,
807 Carminati, E., Ferrarin, C., Fofonova, V., Nicholls, R., Rubinetti, S., Rubino, A., Sannino, G., Spada, G.,
808 Thiéblemont, R., Tsimplis, M., Umgiesser, G., Vignudelli, S., Wöppelmann, G., and Zerbini, S.: Review
809 article: Sea-level rise in Venice: historic and future trends, *Nat. Hazards Earth Syst. Sci. Discuss.*, 1–56,
810 <https://doi.org/10.5194/nhess-2020-351>, 2020.

811

812

813 **Appendix A**

814 Here we present the equations and the graphical results of the theoretical ESL scenarios. TWL results from the
 815 combination of storm surge, tide, and waves components, each following a general functional form (i.e.
 816 harmonic component) describing the oscillation of water level, following trigonometric functional forms for
 817 each component. The equations are given as follows.

$$T_l = T_{max} \times \cos\left(2\pi \frac{1}{T_p}(t + T_d + T_p)\right) \quad \text{Eq. A1.1}$$

818 Where T_l is the tide level in meters at any given time, T_{max} is the maximum tide level in meters, T_p is the tidal
 819 period in seconds, T_d is the tidal period shift in time in seconds (used to match the peaks of tides and storm
 820 surge events), and t is the time in seconds.

$$SS = SS_{max} \times 0.5 \times \left(1 + \cos\left(2\pi \frac{1}{S_p}(t + S_d + S_p)\right)\right) \quad \text{Eq. A1.2}$$

821 Where SS is the storm surge level in meters at any given time, SS_{max} is the maximum storm surge level in
 822 meters, S_p is the storm surge duration in seconds, S_d is the storm surge shift in time in seconds (used to match
 823 the peaks of tides and storm surge events), and t is the time in seconds.

$$W_{c,int} = 0.5 \times \left(1 + \cos\left(2\pi \frac{1}{S_p}(t + S_d + S_p)\right)\right) \quad \text{Eq. A1.3}$$

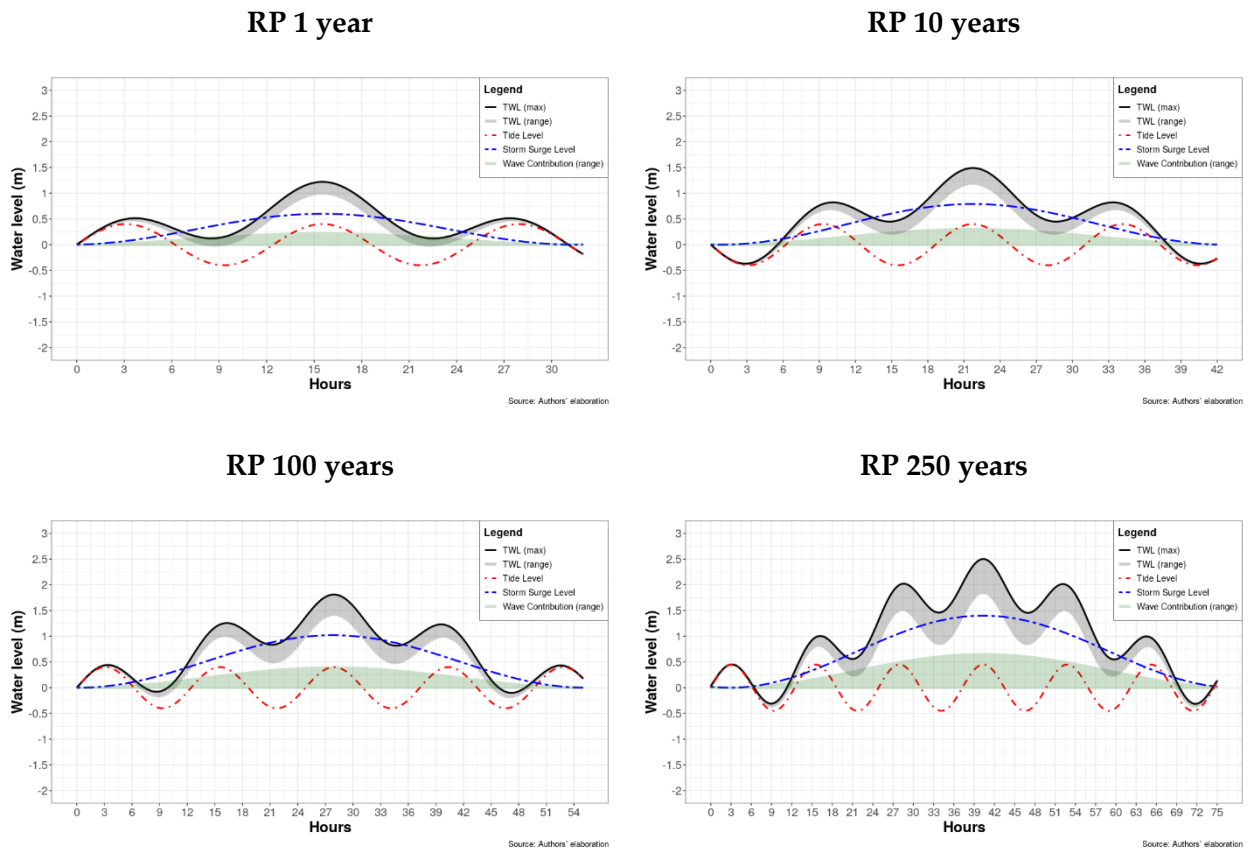
$$W_c = W_{max} \times 0.5 \times \left(1 + \cos\left(2\pi \frac{1}{W_p}\left(t + \frac{W_p}{4}\right)\right)\right) \times W_{c,int} \quad \text{Eq. A1.4}$$

824 Where W_c is the wave contribution in meters at any given time, W_{max} is the maximum wave setup level in
 825 meters, W_p is the wave period in seconds, $W_{c,int}$ is the intensity factor [0-1] of the wave contribution event as
 826 a function of the storm surge intensity, S_p is the storm surge duration in seconds, S_d is the storm surge shift in
 827 time in seconds (used to match the peaks of tides and storm surge events), and t is the time in seconds.

828 We consider the wave contribution component near-shore as a function of the intensity of the storm surge
 829 level, as shown in Eqs. A1.3 and A1.4. As such, the action of waves is simulated as a composite function, where
 830 the maximum wave contribution level is designed to coincide in time with the maximum storm tide level, and
 831 the directions of the waves are set to coincide with the direction of the storm surge event, in our case,
 832 perpendicular to the coastline. This is done first to follow the assumption of worst-case scenario, and second
 833 to incorporate the flood dynamics resulting from the momentum of waves directed inlands. The composite
 834 function that combines Eqs. A1.1 to A1.4 and the effects of VLM and MSL (e.g. due to SLR) is shown in Eq.
 835 A1.5. The results of each component in Eqs. A1.1 to A1.4 and for each probabilistic scenario are shown in
 836 Figure A1.

$$TWL = MSL + VLM + T_l + SS + W_s \quad \text{Eq. A1.5}$$

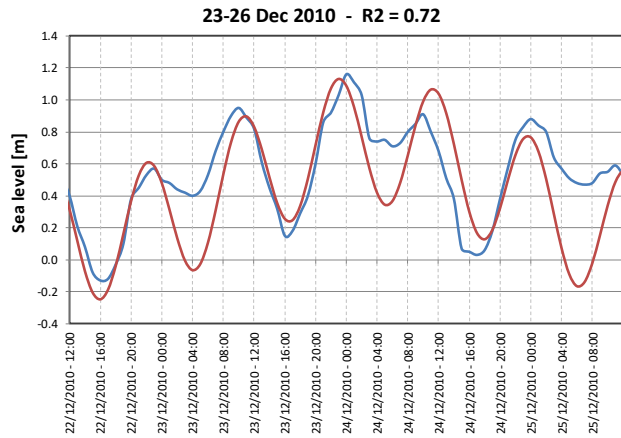
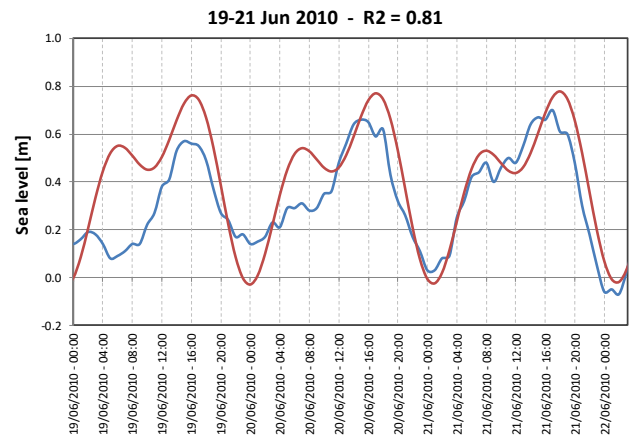
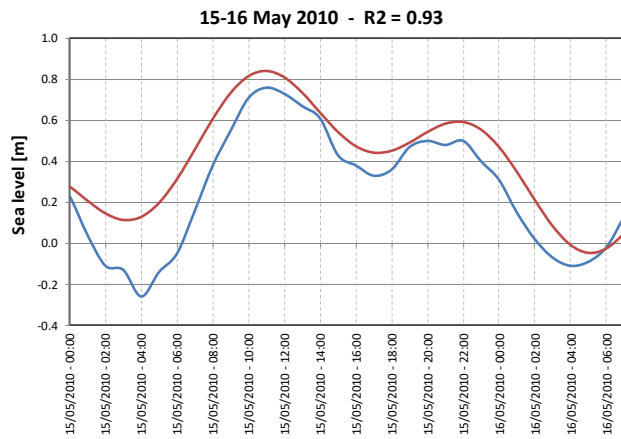
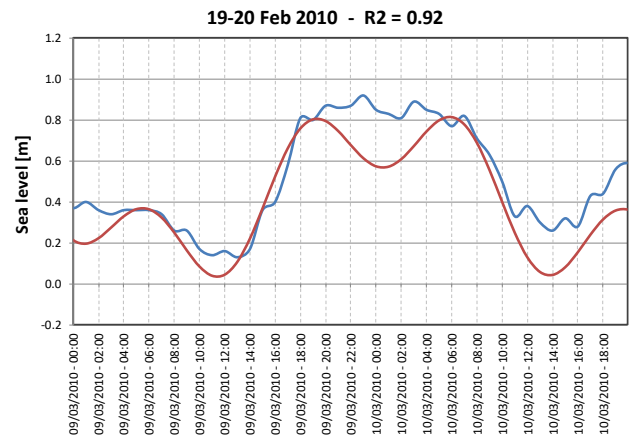
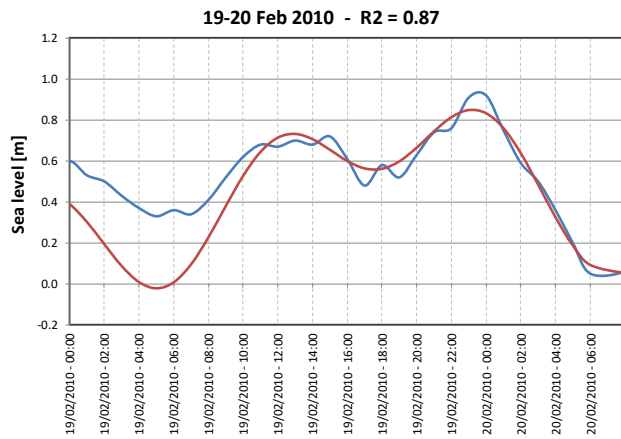
837



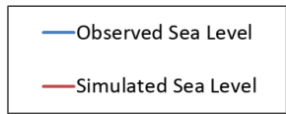
838 **Figure A1.** Dynamic boundary conditions for simulating theoretical extreme sea level events in ANUGA. The
 839 Total Water Level is show as the grey shaded area, while the maximum Total Water Level is shown by the
 840 black line, at any given time. The tide (dashed red line), storm surge (dashed blue line) and wave contribution
 841 (green shaded area) components define the total water level. Configurations are shown for the return periods
 842 of once-in-1, 10, 100 and 250 years.

843 In order to verify the applicability of the aforementioned functions, we test the methods explained in this
 844 Appendix for all five ESL events that were observed along the coastline of the ER region during the year 2010,
 845 as reported in Perini et al. (2011). Observed sea level data is obtained from ISPRA, for the station Ravenna –
 846 Porto Corsini (Rete Mareografica Nazionale, 2021). We evaluate the goodness-of-fit of the methods by means
 847 of Coefficient of determination (R^2). The results of this analysis are shown in Figure A2 below.

848



Extreme events - 2010					
	19-20 Feb 2010	09-10 Mar 2010	15-16 May 2010	19-21 Jun 2010	23-26 Dec 2010
MSL (m)	0.15	0.15	0.15	0.15	0.15
Tmax (m)	0.20	0.20	0.20	0.20	0.40
SS (m)	0.50	0.50	0.40	0.40	0.45
Ws (m)	0.12	0.12	0.14	0.14	0.15
Time (h)	32	34	32	25	72

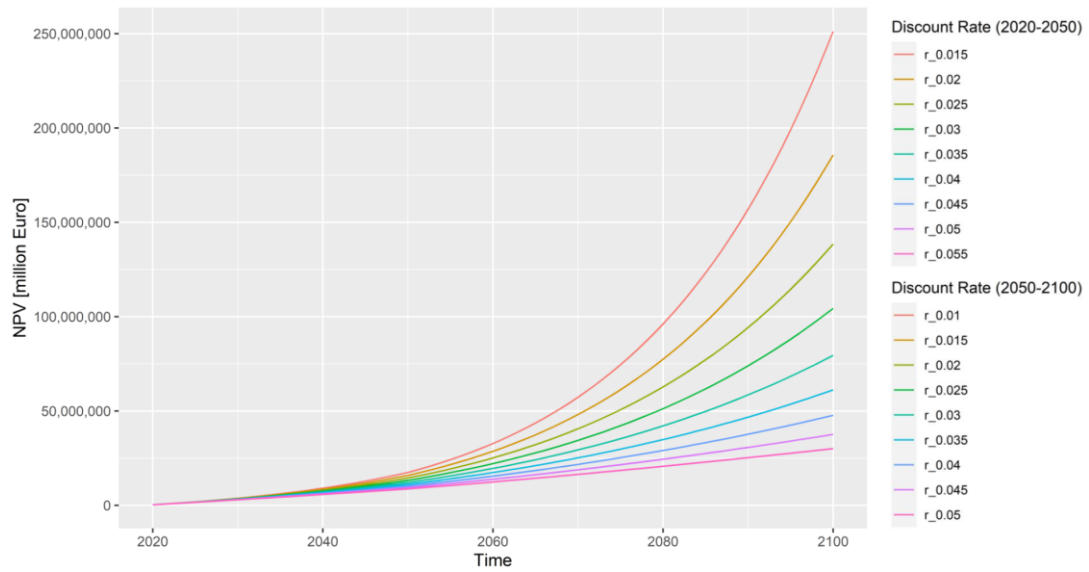


849 **Figure A2.** Comparison of the observed sea level (in blue) versus the simulated sea level using the harmonic
 850 components (in red).

851

852 **Appendix B**

853 A sensitivity analysis is carried out on the discount rate. Figure A2 below shows how the NPV changes with
854 discount rate r ranging from 1.5% to 5.5% (2020 to 2050) and 1% to 5% (2050-2100).



855

856

Figure B1. Sensitivity analysis of NPV using a variable discount rate.